CHALMERS
UNIVERSITY OF TECHNOLOGY

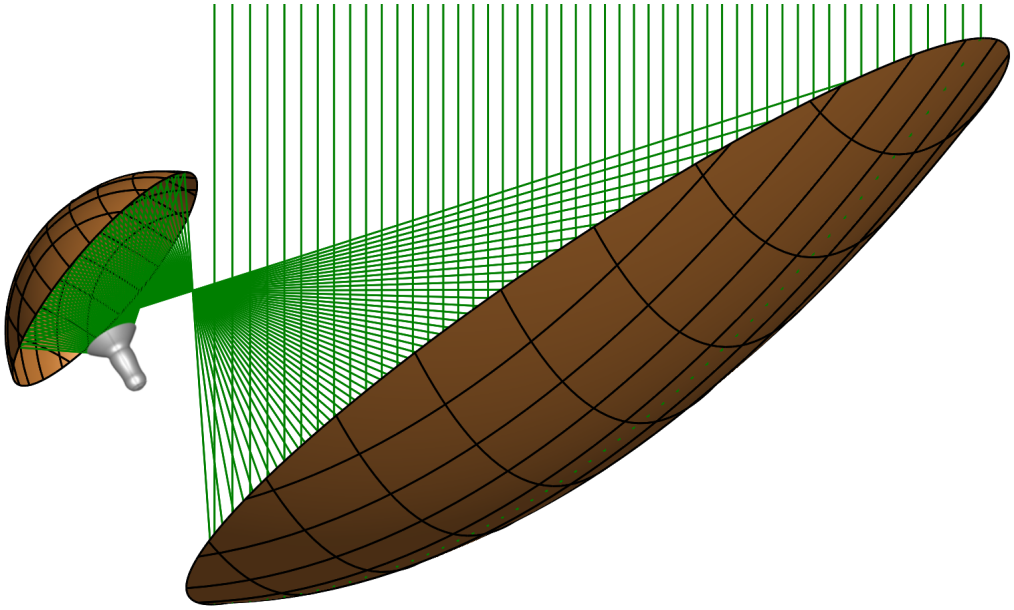

A Wideband Quad-Ridge Flared Horn Feed Design for the Square Kilometre Array Band 1

Antenna Design, Simulation and Measurement

Master's thesis in Fundamental Physics

JONAS FLYGARE

Department of Earth and Space Sciences
CHALMERS UNIVERSITY OF TECHNOLOGY
Gothenburg, Sweden 2016

I'm a Hail Mary pass on homecoming night
Six points down with the clock ticking by
Come hell or high water I still believe I can win
Just call me the comeback kid

Kip Moore

Master's thesis

A Wideband Quad-Ridge Flared Horn Feed Design for the Square Kilometre Array Band 1

Antenna Design, Simulation and Measurement

JONAS FLYGARE

CHALMERS
UNIVERSITY OF TECHNOLOGY

Department of Earth and Space Sciences
Chalmers University of Technology
Gothenburg, Sweden 2016

A Wideband Quad-Ridge Flared
Horn Feed Design for the
Square Kilometre Array Band 1
Antenna Design, Simulation and Measurement
JONAS FLYGARE

E-mail: jonas.flygare@chalmers.se; jonas.b.flygare@gmail.com
Phone: +46 (0)73 981 6912

Supervisors: Dr. Miroslav Pantaleev and Dr. Bhushan Billade, Earth and Space Sciences, Onsala Space Observatory
Examiner: Prof. Gunnar Elgered, Earth and Space Sciences, Onsala Space Observatory

Master's Thesis
Department of Earth and Space Sciences
Chalmers University of Technology
SE-412 96 Gothenburg
Telephone +46 (0)31 772 1000

Onsala Space Observatory
SE-439 92 Onsala
Telephone +46 (0)31 772 5500

Cover: Illustration of a Quad-Ridge Flared Horn feed illuminating an offset Gregorian reflector geometry.

Typeset in LaTeX
Gothenburg, Sweden 2016

A Wideband Quad-Ridge Flared Horn Feed Design
for the Square Kilometre Array Band 1
Antenna Design, Simulation and Measurement
Jonas Flygare
Department of Earth and Space Sciences, Onsala Space Observatory
Chalmers University of Technology

Abstract

The vast and unimaginable greatness of the universe will never stop to amaze us humans. A strive to know, explore or just to grasp the concept of space will always drive us, both philosophically and technically. As a result of this, the visions and advances in radio astronomy for the foreseeable future are very optimistic and a significant part of this will be realized in the Square Kilometre Array project (SKA). The objective is to create the world's largest radio telescope array through interferometry with thousands of telescopes in the deserts of Australia and South Africa. A portion of these will be designated to single-pixel feeds on Gregorian offset reflector dishes. The band covering $350 - 1050$ MHz is defined as SKA Band 1 and is within the region of the general Ultra High Frequency (UHF) band. This is a very challenging area in radio astronomy due to the great amounts of radio-frequency interference (RFI) from cellphones, television broadcast and global navigation satellite systems (GNSS) at these frequencies. To minimize interference we require radio silent environments, and to account for other environmental effects such as the atmosphere and cosmic radiation, we need high-level optimized systems. This combination enables us to detect weak outer space sources with a radio telescope.

We show the development of a wideband Quad-Ridge Flared Horn (QRFH) feed for Band 1 and how it fulfills our specified requirements. We discuss the properties of the QRFH and focus on the trade-off in reducing spill-over together with a high aperture efficiency on an offset dual reflector. For the lower end of the frequency band in focus, there is a strong contribution of noise from the sky, which increases the challenges in the system design. The main objective, which is high sensitivity, is achieved with an average $A_{eff}/T_{sys} > 4.2$ m^2/K across the $3:1$ frequency band and an input reflection better than -10 dB.

Development of the feed is largely based on stochastic optimization with parametrized QRFH feed models. The customizable spline horn profile and the power of genetic algorithms is explained with an emphasis on particle swarm optimization (PSO). We also briefly mention the transfer of the electromagnetic design of the feed, into a mechanical prototype which was finished early in 2016. In late June the same year it was shipped to Penticton, Canada and the Dominion Radio Astrophysical Observatory (DRAO) where it was mounted on the DVA-1, an early prototype reflector for the SKA. At 11.30 AM Pacific Standard Time (PST) on the 22$^{\text{nd}}$ of June 2016, we received first light with a sweep over the radio source Cassiopeia A.

Keywords: antenna, feed, wideband, square kilometre array, quad-ridge flared horn, offset gregorian dual reflector, radio astronomy, stochastic optimization, genetic algorithm.

Acknowledgements

First of all I would like to thank my supervisors Dr. Miroslav Pantaleev and Dr. Bhushan Billade for giving me this opportunity alongside with my examiner Prof. Gunnar Elgered who has been very supportive during this time. Thank you to all of you, including Dr. Peter Forkman, for giving me the chance to start my career at Onsala Space Observatory and to Prof. John Conway for showing continued faith in me and my work.

I would like to express my big love and gratitude for my parents. Mom and Dad, you have always supported me and there have been plenty of times, especially during this work, I have needed and appreciated all the motivation and strength you give me. Thank you to my entire family for always believing in me.

A special shout-out to all the people at the AQP laboratory and MC2 for letting me spend most of my waking hours there for the last two months while finishing this thesis. I owe what feels like a boatload of coffee to you guys. Tobias and Sofia deserve more than a thank you for putting up with me for this long.

Thank you to the entire team of colleagues in Onsala for making the observatory a fun, interesting and more often than not, quite a peculiar place to work. I look very much forward to continue this everyday journey and the sometimes unforgettable lunch break discussions.

I would also like to express my gratitude to Dr. Astrid Algaba Brazález, Prof. Jian Yang and Prof. Per-Simon Kildal for giving me the internship opportunity that really sparked my interest for the field of antennas. You trusted me to work with you, and all the great people at the Antenna Group at Chalmers, which paved my way into this exciting field.

Last but not least to all my friends; thank you for always being there, especially Jim, Martin, Johan, Vespera, Linda, Courtney, Tobias and Sofia.
It has been a long road, but you didn't lose faith in this comeback kid.

Jonas Flygare, Gothenburg, November 2016

Contents

List of Figures

1
Introduction

The strive to explore the world around us and the fascination of the deep unknown of space will always be a trait of mankind. To study the earth, the solar system and beyond is a curiosity starting from just looking up onto the night sky and wonder what is out there. The field of Astronomy dates back to civilizations as early as the Babylonian, Egyptian, Mayan and several other where the first observations were simple studies of the night sky [1]. The natural course of history is to improve and the way to improve astronomical observations is the telescope. The first ever recorded telescope was constructed in 1608 by Hans Lippershey [2], who filed an unsuccessful patent application in the Netherlands for his design. This was of course a "classic" refracting optical telescope which is basically a large monocular based on a classic lens. Based off of the limited descriptions of this design, Galileo Galilei finished his first telescope, from two lenses and an organ pipe, one year later. Fast forwarding to the modern day professional astronomy the refracting telescope has been replaced by the radio telescope where electromagnetic waves radiated from distant sources in the universe are observed and analyzed. Large parabolic reflector antennas that collect waves at radio frequencies is a technique greatly utilized by astronomers. By observing the electromagnetic waves of an object far out in space, knowledge about element composition, distance, velocity and much more can be extracted.

1.1 Interferometry

A powerful technique in radio astronomy is called interferometry [3] where several antennas are probing the same distant electromagnetic source and then correlating the data from different antennas with a very precise time-stamp of when the signal was received. A set of antennas can in this way form an array where they are working together as a single antenna and the angular resolution and detail of the source object is greatly enhanced. In fact; using two reflector antennas, with a certain dish diameter, separated 100 m in distance would correspond to having a single reflector antenna with a 100 m diameter. Even though a large single dish would increase the total amount of power collected, it is easy to see why it is more advantageous to build several smaller reflector dishes for practical reasons. The core of a reflector antenna is the directional feed situated at the focus point for the incoming electromagnetic waves. This is where the waves are collected and sent towards the back-end of the receiving system, as a signal, for amplification and processing. The properties of the reflector antenna are dependent on both the design of the reflector dish and the feed.

1.2 Square Kilometre Array

The Square Kilometre Array (SKA) project [4] is an international collaboration for the construction of the world's largest radio telescope array with an effective total collecting area of one square kilometre. Fully operational, the SKA telescope will be the most powerful telescope ever constructed with a resolution even better than the Hubble telescope [5] which is situated outside the earth's protective (and clouding) atmosphere. This improvement in observation technology will open the science door to explore a great many areas. A few examples of these are using cosmic pulsars as gravitational detectors for major tests of Einstein's general relativity theory, dark matter and dark energy exploration and even the search for extra-terrestrial life.

1.2.1 SKA1 - Baseline

The frequencies to be covered in the first and second phase of SKA spans more than two decades in frequency and ranges from 50 MHz to 13.8 GHz. For such a wide span different array technology [6] is needed for optimal performance across different frequency bands. The lower frequencies $50 - 350$ MHz will be covered in SKA-low by phased aperture arrays that will be located in Australia. SKA-survey will include 350 MHz to 4 GHz with a multi-beam feed in a dual reflector phased array system. The dual reflector array system of the SKA-mid, to be located in South Africa, ranges currently from 350 MHz to 13.8 GHz where five wideband single pixel feeds are designed to cover the frequency span. The lowest band in the SKA-mid, therefore the physically largest single pixel feed, is defined as SKA Band 1, $350 - 1050$ MHz.

1.3 Scope of Thesis

The content of this work is the design and optimization process of a proposed Quad-Ridged Flared Horn (QRFH) feed for Band 1 frequencies of the SKA, in an offset Gregorian dual reflector geometry. The feed design work was done at Onsala Space Observatory (OSO) [7]. Due to the majestic complexity of an entire radio telescope system (back-end, low noise amplifiers (LNA), control systems, mechanical construction etc.) the thesis is strictly including the feed design and its performance on-dish. Short parts of the thesis are addressing the transformation from an electromagnetic design to the mechanical counterpart. This will include some comparison of simulations to prove that the electromagnetic performance is consistent in the mechanical design as well as measurements on the prototype. The entire system is of great interest to the author (paper A.1), but would well enough cover more than a few master thesis's. The theory part of the thesis will therefore strictly include relevant topics to this project and the specific antenna technology used. This will also be the case for the evaluation, specifications and properties introduced, again to restrain the size of the thesis.

1.3.1 Software

During the project several different softwares have been utilized for simulation and data processing. The main optimization was performed with the designated feed optimizer [11] and further evaluation through the system simulator [12] both supplied by Prof. Marianna Ivashina at the Antenna Group, Department of Signals and Systems at Chalmers University of Technology. These software packages are executed through MATLAB [13], CST Microwave Studios [14] and GRASP [15], where MATLAB handles the control process, data and statistical analysis whilst CST serves as the electromagnetic design and simulation tool. GRASP is the main tool for on-dish simulation of the feed performance. For cross evaluation of the feed performance and analysis, FEKO [16] and HFSS [17] have been used as well however these results are not presented here. The process of design and optimization methods used is explained in Chapter 4.

1.3.2 Conventions

The intention is to keep consistent conventions in figures and definitions as much as possible. The field of antennas suffers sometimes from mixtures of official and personal definitions and references, and this causes confusion. Chapter 2 is therefore intended to give a theoretical base on some key concepts. Please note in Chapter 5 that unless stated otherwise, green curves represent what is defined as ”vertical” polarization on the telescope and port 1 (x-polarization) on the feed. Black curves represent the ”horizontal” polarization on the telescope and port 2 (y-polarization) on the feed. When representing simulated and measured results the convention of using dashed line for the former and solid for the latter is most often the case. However, when co- and cross-polarization is represented this notation is also used in other form. Dashed lines and other forms of lines could also be used for separation of several curves with similar meaning. It is very important to read the figure text and figure legends for the correct interpretation in each individual case. It is assumed that knowledge of the spherical coordinate system is routine to the reader. A common mix up in the description of angle in the sky relative the horizon is the mentioning of elevation compared to zenith angle. *Elevation* or *altitude* denotes the angle 0° at the horizon and zenith as 90°. The *zenith angle* defines the horizon as 90° and zenith as 0°. We will in almost all cases use the zenith angle, in the thesis denoted as θ_p, especially when discussing the telescope pointing direction. For clarity, zenith direction is along the vector which is orthogonal to, and is pointing out from, a local horizontal plane on the earth’s surface. When θ is used, it is most often referring to the spherical coordinate when defining the base coordinate system for the far-field function.

2

Antenna Theory and Astronomy

This section is based on well known antenna and reflector theory found in excellent books such as [18], [19], [20] and [21]. We present basic tools for understanding electromagnetism in the field of antennas in general as well as the specific focus on Quad-Ridge Flared Horns and Gregorian offset reflectors. The purpose of this section is to form the base of the project, which can be easily referenced to explain the analysis and results in the later parts of this thesis. Due to different definitions used around the antenna community we will rely on the definitions given by the IEEE standards [22], unless stated otherwise. However, we will start off this section with an important concept in radio astronomy.

2.1 Brightness Temperature

In radio astronomy it is common to characterize radiation from a source in terms of a *brightness temperature*. This temperature, $T_b(L, f)$, is related to the spectral radiance, $L(f, T_b)$, and frequency, f, through Planck's law of classic black-body radiation

$$L(f,T) = \frac{2hf^3}{c^2}\frac{1}{e^{\frac{hf}{k_B T_b}} - 1} \qquad \left(\frac{\text{Jy}}{\text{sr}} \cdot 10^{26}\right) \tag{2.1}$$

where k_B is the Boltzmann constant, h is the Planck constant and c is the speed of light. For the Rayleigh-Jeans limit at low frequencies or high temperatures, i.e. $f << k_B T_b/h$, a series expansion of Equation 2.1 gives us the spectral radiance and brightness temperature as

$$L(f,T_b) \approx \frac{2k_B f^2 T_b}{c^2} \qquad \left(\frac{\text{Jy}}{\text{Sr}} \cdot 10^{26}\right) \tag{2.2}$$

$$T_b(L,f) = \frac{Lc^2}{2k_B f^2} = \frac{L\lambda^2}{2k_B} \qquad (\text{K})\,. \tag{2.3}$$

The brightness temperature $T_b(L, f)$ is the physical surface temperature of a black body in thermal equilibrium if it produces the spectral radiance $L(f, T_b)$. A perfect black body absorbs all incoming electromagnetic radiation and it is also characterized by showing spectral radiance at a higher or equal level to any other type of body. This means that a non-black body object would measure a lower brightness temperature than its actual surface temperature. This defines the *emissivity*, ϵ, of an object as

$$T_b(L, f) = T_p\epsilon \tag{2.4}$$

where T_p is the physical body temperature. It is important to distinguish the brightness temperature from a real physical temperature of an object in this thesis. Both temperatures occur when we discuss the noise temperature (Section 2.2.8) of the antenna.

2.2 Antenna Properties

Several properties described here are applicable in many other areas and are not antenna specific. For the purpose of the thesis we try to keep the specific equations showed here as applicable as possible to the project and radio astronomy. We will use the zenith angle denoted as θ_p for the angle in the sky, as defined in Section 1.3.2.

2.2.1 Reciprocity

The reciprocity of antennas is fundamental in the understanding of this section. It states that the properties of an antenna in transmit mode, are identical to the properties of the same antenna as a receiver. This means that if we know how the antenna radiates in one mode of operation, we also know the reverse mode. The proof of this will be left as an exercise to the very enthusiastic reader [23]. There are exceptions with real antennas where reciprocity does not apply. Throughout this thesis, all antennas are linear and reciprocity is assumed.

2.2.2 Plane Wave Approximation

A radiating source or antenna, would emit a spherical wave spreading in all directions. At a very large distance from the radiating object, let us say the distance between a star and an earth-located telescope, the spherical waves can be approximated to be planar. This is a simplification to make the calculations easier but is of course not physically valid, since such a planar wave would require infinite power. We will not go into further details of this and the enthusiast should consult the textbooks referenced at the beginning of the chapter.

2.2.3 Bandwidth

In general the bandwidth is the difference between the lowest and highest frequency in a system's given span of operation, i.e. $\Delta f = f_H - f_L$, with the lowest frequency in the band defined as f_L and the highest frequency as f_H. This defines the center frequency as $f_C = (f_H + f_L)/2$ and we can express the bandwidth in percentage as

$$\%B = 100\frac{f_H - f_L}{f_C} = 200\frac{f_H - f_L}{f_H + f_L} \qquad (\%)\,. \tag{2.5}$$

However, for a wideband antenna we will define the bandwidth conventionally as a ratio according to

$$B = \frac{f_H}{f_L} \tag{2.6}$$

which is expressed as $B : 1$ bandwidth.

2.2.4 Beam Pattern

General electromagnetic field theory will be left out of this thesis and is assumed to be well known. We will briefly note the *far-field* region, which means that at a distance larger than $2L_D^2/\lambda$ from the antenna, the E-field and H-field are separable into components. Here λ is the wavelength and L_D is the largest dimension of the antenna, effectively the aperture diameter. With a phase component e^{-jkr} and a decay inversely proportional to the distance r from the antenna we can write the E-field as

$$\mathbf{E}(r, \theta, \phi) = \frac{e^{-jkr}}{r}\mathbf{G}(\theta, \phi) \tag{2.7}$$

where $\mathbf{G}(\theta, \phi)$ is the *far-field function* which defines the direction and phase of the field. We will later discuss the *phase center* which minimizes the phase variation of the wave-front and maximimes the phase center efficiency if located at the reflector antenna focal point.

2.2.5 Polarization

We can define antenna polarization as the two far-field components *co-polarization* and *cross-polarization*, where the former is the desired polarization. For a linearly polarized antenna in a spherical coordinate system, this is convenient to do with Ludwig's 3^{rd} definition [24] that gives base vectors for x- and y-polarization according to

$$\begin{aligned} \hat{\mathbf{x}} &= \cos\phi\hat{\boldsymbol{\theta}} - \sin\phi\hat{\boldsymbol{\phi}}, \\ \hat{\mathbf{y}} &= \sin\phi\hat{\boldsymbol{\theta}} + \cos\phi\hat{\boldsymbol{\phi}}. \end{aligned} \tag{2.8}$$

When discussing the cross-polarization ratios of dual-polarized antennas, the *intrinsic cross-polarization ratio*, IXR, can be used as a figure of merit for the polarization performance of the system [25]. Polarization purity will not be discussed in any detail in this thesis, but the values calculated from the Jones matrix will be shown as part of the requirement.

2.2.6 Gain

Antenna gain or simply *gain*, G, is defined as the ratio of the radiating intensity in a given direction of the antenna, to the intensity of an isotropically radiating antenna [22]. G does not include mismatch losses from impedance or polarization, and should be considered independently of the back-end system it is connected to.

If the antenna would not suffer any dissipative losses the gain would be equal to the so called directivity, D. However, the case of a loss-less antenna is not realistic so we define the relation according to

$$G = \eta_{dis} D \tag{2.9}$$

where η_{dis} is the linear efficiency reducing the gain due to dissipative losses (ohmic, etc.). If we include the losses from the impedance mismatch as well in the antenna we would have to include another efficiency, η_{mis}, which would give us the *realized antenna gain* or simply *realized gain* as

$$G_{real} = \eta_{dis}\eta_{mis} D. \tag{2.10}$$

G_{real} is, unlike G, dependent on the back-end system which it connects to, and $\eta_{mis} = 1 - |\Gamma_A|^2$ where Γ_A is the magnitude of the linear reflection coefficient at the antenna port. The combined efficiency $\eta_{dis}\eta_{mis}$ is defined as the *realized radiation efficiency* or more commonly *total radiation efficiency* of the antenna, $\eta_{rad} = \eta_{dis}\eta_{mis}$. To distinguish between directivity and realized gain, we could say that directivity is the theoretically radiated power from the antenna that we calculate assuming no losses. The realized gain is the radiated power we actually measure with the losses unavoidably included. Theoretical calculations of the realized gain are very difficult and therefore measurements are crucial to estimate the total radiation efficiency. For a directional antenna the gain is typically referring to the pointing direction, which should be the maximum gain. Equations 2.9 and 2.10 are often confused in the literature and sometimes include the polarization efficiency η_{pol}. The polarization mismatch is defined as the ratio of the received power from an arbitrary plane-wave in an antenna to the power received by the antenna from the same plane-wave but with the polarization adjusted to give the maximum possible power received.

2.2.7 Antenna and Aperture Efficiency

An electrically large antenna with a physical aperture in which the radiation passes through (or is collected with, e.g. a reflector antenna) is called an *aperture antenna*. To define how effectively this physical area is used we define a ratio of the maximum effective area to the *physical area*, A_{phy}, which is called *antenna efficiency* according to

$$\eta_{ant} = \frac{A_{eff}}{A_{phy}} \tag{2.11}$$

The maximum *effective area*, A_{eff}, is the ratio of the power, P, available at the terminals of the antenna to the power flux density, W, of a plane wave incident to the antenna in that direction with the wave being polarization matched to the antenna. For a given direction and frequency, the effective area is also defined by the wavelength λ and the antenna gain as

$$A_{eff} = \frac{P}{W} = \frac{\lambda^2}{4\pi} G \qquad \left(\mathrm{m}^2\right). \tag{2.12}$$

The ratio between the directivity, D, from a planar aperture and the *standard directivity*, D_{ref}, from the same planar aperture but excited with a uniform-amplitude and equal-phased distribution, is called the *(aperture) illumination efficiency*

$$\eta_a = \frac{D}{D_{std}}. \tag{2.13}$$

For a planar aperture where $A_{phy} >> \lambda^2$, the standard directivity takes the value $D_{std} = 4\pi A_{phy}/\lambda^2$ where A_{phy} is the aperture area. If we insert this into Equation 2.13 we get

$$\eta_a = \frac{\lambda^2}{4\pi}\frac{D}{A_{phy}}. \tag{2.14}$$

η_a is commonly confused with η_{ant}, since they are not always related in an obvious way. We rearrange Equation 2.14 as

$$D = \frac{4\pi A_{phy}}{\lambda^2}\eta_a \tag{2.15}$$

and combine with Equations 2.9 and 2.12, after some further rearranging we end up with

$$\frac{A_{eff}}{A_{phy}} = \eta_a \eta_{dis}. \tag{2.16}$$

If we compare the Equations 2.16 and 2.11 we see that

$$\eta_{ant} = \eta_a \eta_{dis}. \tag{2.17}$$

This is a valid result, considered in context with what type of antenna system that is described, as well as the current plane of reference. In the case of a single feed horn η_a and η_{ant} keeps a simple form, but when we include a reflector dish in the system several other sub-efficiencies will characterize the result [26]. Contributions both from the dish itself, and the feed performance relative the dish is then included. We will discuss these efficiencies more in Section 2.3.1 when we consider parabolic reflectors.

2.2.8 Noise Temperature

One of the fundamental objectives when designing an antenna system is to minimize the unwanted noise. The contributions from surroundings as well as the noise from components needs to be minimized in order to maximize the signal-to-noise ratio (SNR) at the output. These contributions are further discussed in Section 2.4. The concept of *noise temperature* is a way of expressing the temperature equivalent of the noise power present in a system. According to the Johnson-Nyquist relation we can express the noise power per unit bandwidth as

$$\frac{P}{\Delta f} = k_B T_n \qquad (\mathrm{W} \cdot \mathrm{s}) \tag{2.18}$$

where P is the power, $\Delta f = f_H - f_L$ the bandwidth, k_B the Boltzmann constant and T_n is the equivalent noise temperature. For a perfect black body we would have a noise contribution $T_n = T_p$, but the more realistic case was shown in Equation 2.4. To clarify the meaning of noise temperature, we give a short simplified example. Assume a source radiating power, P_s, and assume that the power per unit bandwidth is uniform, so the power in the entire band from the source is $P_s = k_B T_b \Delta f$, where T_b is the brightness temperature of the source. At the antenna port the received power is $P_a = k_B T_n \Delta f$, where T_n is the noise temperature. To calculate the power P_a, we would need to know the A_{eff} and power flux density W_s incident from the source at the antenna aperture. For simplicity assume that the source and antenna are ideal isotropic radiators, then $W_s = P_s/(4\pi R_s^2)$, where R_s is the distance from the object to the antenna. According to Equation 2.12, $A_{eff} = \lambda^2/(4\pi)$ since G is unity for an isotropic radiator, this gives us

$$P_a = A_{eff} W_s = \frac{\lambda^2}{4\pi} \frac{P_s}{4\pi R_s^2} = \left(\frac{\lambda}{4\pi R_s} \right)^2 P_s \tag{2.19}$$

where $(4\pi R_s/\lambda)^2$ is the *free-space attenuation*, L_P. Equation 2.18 gives us

$$T_n = \left(\frac{\lambda}{4\pi R_s} \right)^2 T_b. \tag{2.20}$$

This is a very simplified example to illustrate the concept, now assume that T_n is the only noise contribution in the antenna, then this would be the *antenna noise temperature* of the system, T_A, which is of course not a realistic scenario.

2.3 Reflector Antennas

The concept of the reflector antenna is to collect as much power from incident waves as possible and focus this power into a point, where the feed is located. There are many different types of reflectors, both symmetric and asymmetric, with and without sub-reflector. When the feed is evaluated in terms of performance on-dish, some of the equations and efficiencies discussed in the previous sections needs to be expanded.

2.3.1 Parabolic Dish Efficiencies

In general when calculating the aperture efficiency for a complete reflector antenna system, both sub-efficiencies dependent on the feed and the dish should be accounted for. The feed dependent properties discussed in Section 2.2.7 is expanded to involve the polarization efficiency, taper illumination of the reflector, spill-over and phase center efficiency. Depending on what dish is used, different sub-efficiencies will contribute in different portions, such as surface errors (RMS), physical blockage from mechanical structures, transparency, pointing jitter and dissipative losses on the dish surface. Without postulating the mathematical expressions for the following sub-efficiencies, we now define the feed aperture efficiency on-dish as

$$\eta_a = \eta_{sp}\eta_{ill}\eta_{pol}\eta_{ph}. \tag{2.21}$$

Here η_{sp} is the spill-over efficiency which expresses how much of the radiated power actually hits the reflector. The rest will be "spilled" power that possible can hit the ground which would give major contributions to the total spill-over noise. η_{ill} is the taper illumination efficiency that defines how well the dish is illuminated relative a uniform illumination distribution. η_{pol} defines the cross-polarization efficiency and η_{ph} is the phase efficiency which defines how the feed phase center is placed relative to the dish focal point. The combination of η_{sp} and η_{ill} is the most interesting part for this thesis due to their mutual dependence. By illuminating the reflector with a high edge taper, η_{ill} will be close to 100 %, but at the same time this will increase the power lost to spill-over. We illustrate this trade-off in Figure 2.1 with equations from the excellent theoretical example on pp. 265 – 267 in [18]. There is clearly a maximum limit for the product $\eta_{ill}\eta_{sp}$ in this case. In Sections 2.4 – 2.4.1 we discuss this trade-off further and the fact that it plays a role in the spill-over noise contribution which is very important during feed optimization.

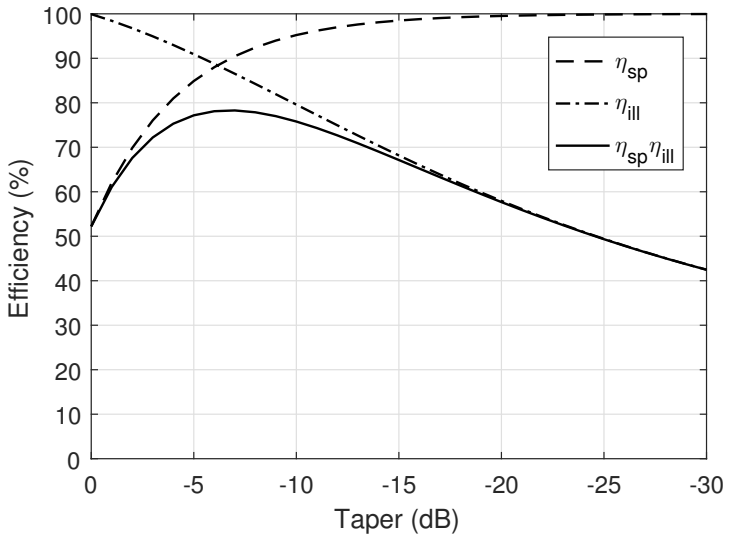

Figure 2.1: Example that illustrates the trade-off between illumination and spill-over efficiency as a product in the aperture efficiency.

Sub-efficiencies for the dish structure itself include η_{block} which defines how much the support structure and feed blocks the aperture. Due to environmental circumstances the telescope would experience small variations in the pointing which is considered in the η_{jitt}. How transparent the dish is to the current frequencies is regarded in η_{trans}, the surface roughness of the dish would be covered in η_{surf} and the dissipative losses of the dish is regarded in $\eta_{disdish}$. We can summarize these efficiencies as the contribution from the dish to the total efficiency as

$$\eta_{dish} = \eta_{block}\eta_{jitt}\eta_{trans}\eta_{surf}\eta_{disdish}. \tag{2.22}$$

With Equation 2.21 and 2.17, we can write an antenna efficiency for the entire telescope system according to

$$\eta_{ant} = \eta_{block}\eta_{jitt}\eta_{trans}\eta_{surf}\eta_{disdish}\eta_{sp}\eta_{ill}\eta_{pol}\eta_{ph}\eta_{dis}. \tag{2.23}$$

Efficiently calculating all these parameters for the system is not a practical approach for our purpose. We are therefore utilizing the physical optics (PO) approximation and calculate A_{eff} for the entire system according to Equations 2.14 and 2.16, see Section 4.3.

2.3.2 Offset Gregorian Reflector Geometry

An offset Gregorian reflector has a main-reflector (MR) which is asymmetric in its shape and resembles more of an ellipse than its symmetric counterpart. This is to compensate for the fact that the sub-reflector (SR) and the feed is offset from the boresight direction which makes the illumination of the dish non-symmetric. The SR has an ellipsoidal shape that focus the power coming from the MR into the feed, see Figure 2.2. The fact that the feed and SR are offset from boresight reduces the physical blockage to a minimum ($\eta_{block} \approx 100$ %). The *half-opening angle* or *half-subtended angle*, θ_e, is an important design parameter and is illustrated in Figures 2.3 and 2.4. The feed is optimized, so that as much power as possible is focused within these limits to maximize illumination and minimize spill-over. Depending on the dish design, there can be an extension on the lower end of the SR, which goes above θ_e. This is advantageous to reduce the spill-over noise pickup from the ground.

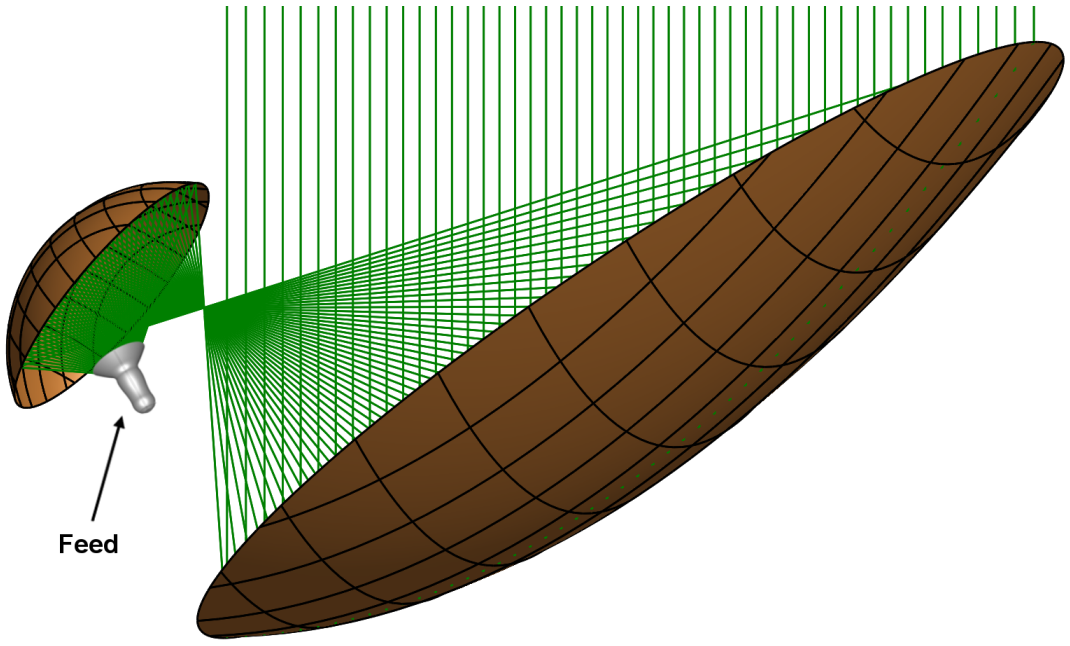

Figure 2.2: Illustration of ray focusing into the feed for an offset Gregorian dual reflector system.

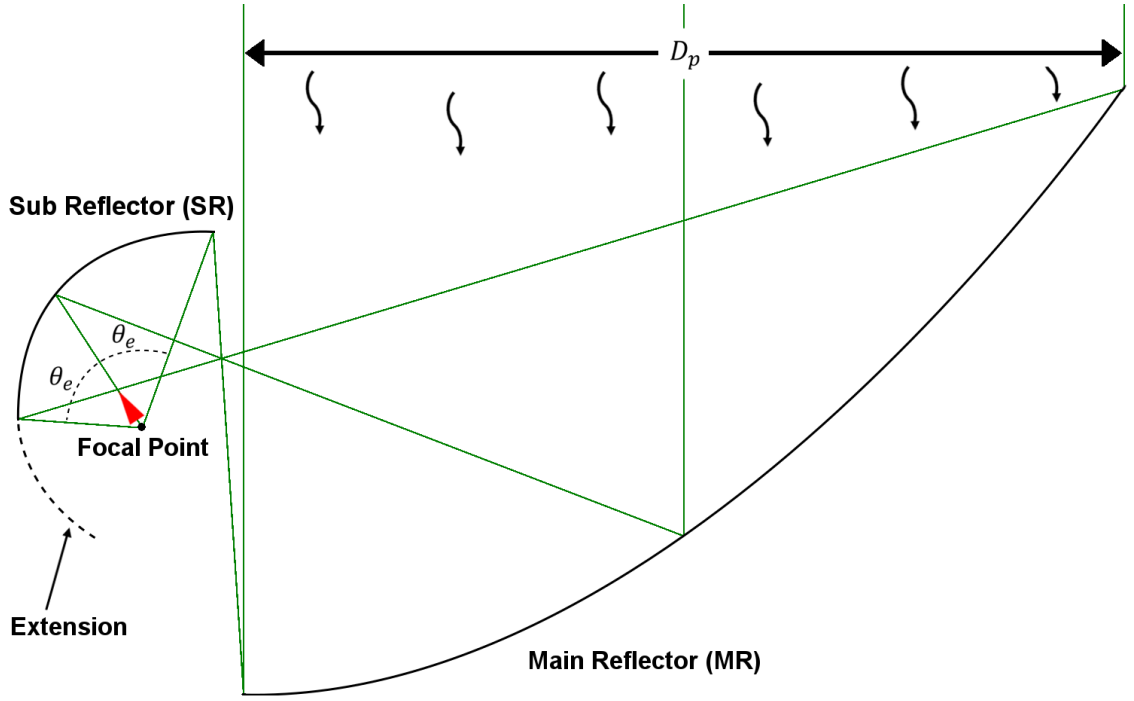

Figure 2.3: Offset Gregorian dual reflector geometry with θ_e half-subtended angle (half-opening angle). Incoming electromagnetic waves (wavy arrows) converge at the focal point (black dot) of the reflector geometry, this is where the feed horn phase center is placed. The feed boresight direction is marked with a red arrow. Ray tracing shows the green rays that hits the edges of the main-reflector (MR) corresponds to the θ_e limits at the sub-reflector (SR).

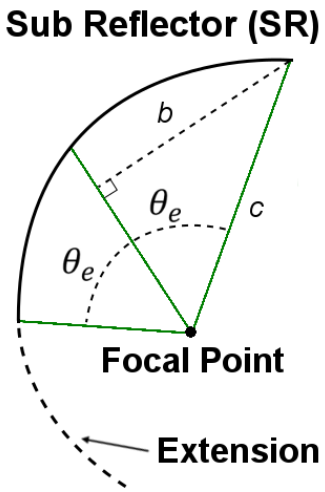

Figure 2.4: Sub-reflector enlarged for the geometry in Figure 2.3. The green rays represent incoming waves converging at the focal point which gives the half subtended angle as $\theta_e = \sin^{-1}(b/c)$.

2.4 System Noise Temperature

A crucial part of most antenna systems, especially in radio astronomy, is to keep the total unwanted noise picked up by antenna as low as possible, to be able to detect the very weak outer space signals. The contributions to the total noise of any antenna system are several and we will discuss the most relevant in a somewhat simplified, but still valid, model. When the telescope is pointing at a certain direction in the sky, for example observing a distant point source like a star, there are several different sources of noise or interference that has to be accounted for. This noise is expressed in terms of a temperature distribution $T(\theta_p, \phi, f)$ defined as

$$T(\theta_p, \phi, f) = \begin{cases} T_s(\theta_p, \phi, f) & 0^\circ \leq |\theta_p| < 90^\circ \\ T_g & 90^\circ \leq |\theta_p| \leq 180^\circ \end{cases} \tag{2.24}$$

where θ_p is the zenith angle (can also be defined with elevation θ), ϕ is the azimuth and f is the frequency. In most cases the variations in azimuth direction can be assumed very small, and therefore each ϕ-cut is considered identical. An illustration of such a cut showing the noise distribution surrounding the telescope, is illustrated in Figure 2.5. It is worth noting that the ground temperature will throughout this thesis be assumed a constant number that is equal to the physical temperature, $T_g = T_{phy} = 290$ K, representing the ground emission. This is a simplified case, depending on the reflectance of the surface, a contribution from scattered incoming radiation will contribute. The full expression for this is complicated, but with some valid assumptions we get an approximate expression $T_g(\theta_p, \phi, f) = (1 - |\Gamma_g|^2)T_{phy} + |\Gamma_g|^2 T_s(\theta_p, \phi, f)$ where Γ_g is the reflection coefficient of the ground surface. Further simplifications for the frequency band of interest and with the environment expected, we will assume $T_g = T_{phy} = 290$ K is a valid model.

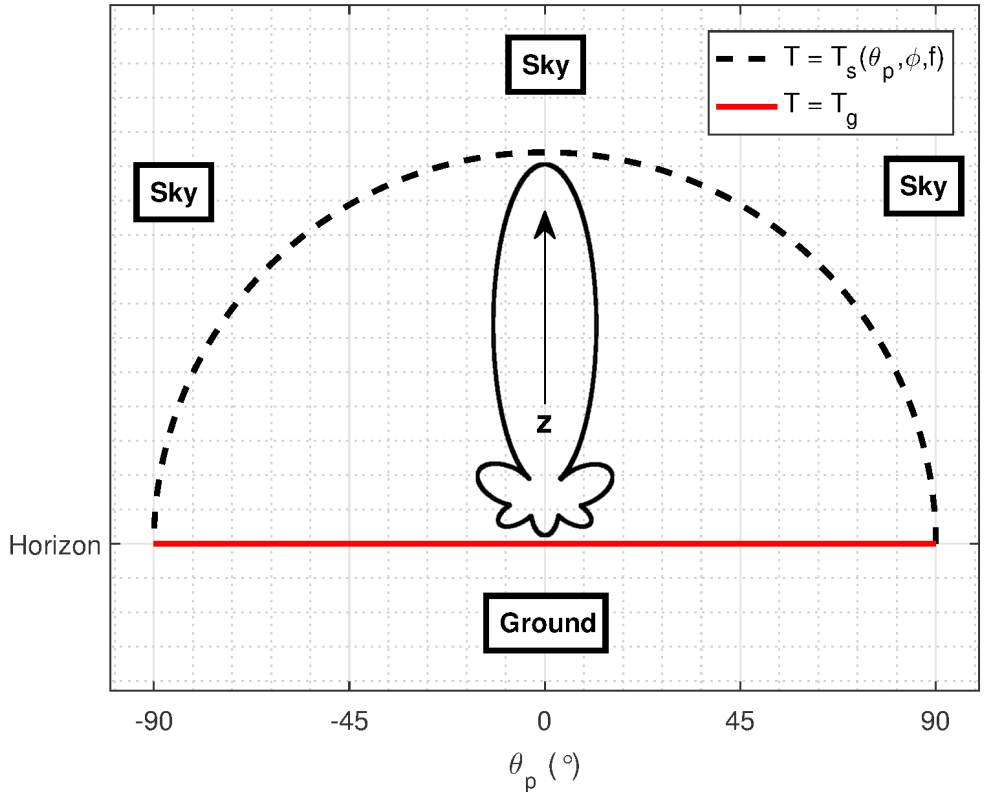

Figure 2.5: Illustration of a noise temperature ϕ-cut surrounding the telescope beam. The black dashed line represents the sky varying in temperature according to $T_s(\theta_p, \phi, f)$ and the red solid line is the constant ground temperature, T_g, in this model. The telescope is pointing in zenith ($\theta_p = 0°$) in this example and the horizontal axis marks the telescope zenith angle if its rotated around the center along the half-circle. The beam pattern is greatly exaggerated and arbitrarily drawn for illustration purposes.

Contributions to the surrounding brightness temperature are the emission from molecules contained in the atmosphere, galactic emission, the cosmic microwave background (≈ 2.7 K) and the emission contribution from the ground. Due to the fact that the telescope will always be looking at the sky, the contribution from the atmosphere and the galactic contributions can only be lowered marginally by spill-over reduction. However, the main source to the spill-over noise is the ground which is around 290 K in temperature and can therefore give a significant contribution. To reduce spill-over noise the telescope system should be optimized to pick up as little of the emission from ground as possible. With $T(\theta_p, \phi, f)$ given according to Equation 2.24 we calculate the total *antenna noise temperature*, T_A, (including spill-over) for a specific direction and frequency according to

$$T_A = \frac{\iint_{4\pi} G(\theta_p, \phi, f) T(\theta_p, \phi, f) \sin\theta_p \, \mathrm{d}\theta_\mathrm{p} \, \mathrm{d}\phi}{\iint_{4\pi} G(\theta_p, \phi, f) \sin\theta_p \, \mathrm{d}\theta_\mathrm{p} \, \mathrm{d}\phi} \tag{2.25}$$

which could be approximated as

$$T_A = T_s\eta_{sp} + T_g(1 - \eta_{sp}) \tag{2.26}$$

where η_{sp} is the spill-over efficiency. Another contribution to the system noise temperature is the *receiver noise temperature*, T_{REC}, which includes the back-end of the receiver and the low-noise amplifiers (LNA). There will also be a contribution from the losses in the feed itself dependent on the physical temperature, T_{phy}. The total *system noise temperature*, T_{sys}, can then be written as

$$T_{sys} = \eta_{rad}T_A + (1 - \eta_{dis})T_{phy} + (1 - \eta_{mis})T_{REC} \tag{2.27}$$

2.4.1 Sensitivity

Figure of merit for an antenna is G/T_{sys}, which translates to A_{eff}/T_{sys} for a reflector antenna. This is the *signal-to-noise ratio* commonly referred to when evaluating the antenna performance and defined as

$$\frac{A_{eff}}{T_{sys}} = \frac{\eta_{ant}A_{phy}}{\eta_{rad}T_A + (1 - \eta_{dis})T_{phy} + (1 - \eta_{mis})T_{REC}} \qquad \left(\frac{\mathrm{m}^2}{\mathrm{K}}\right), \tag{2.28}$$

where Equations 2.11 and 2.27 are used. Higher spill-over efficiency will obviously decrease the spill-over noise contribution in the total system noise and increase sensitivity, as will a higher aperture efficiency η_a, as seen in Equation 2.28. In Section 2.2.7 and 2.3.1 we discussed why there is a balance between high taper illumination efficiency η_{ill}, which increases η_a, and low spill-over noise. Therefore, the optimization for high aperture efficiency and sensitivity can be seen as a trade-off where an optimum point for the specific dish must be found.

2.5 Quad-Ridge Flared Horn

The Quad-Ridge Flared Horn (QRFH) is a robust wideband feed design that offers dual-polarization with a single-ended low noise amplifier (LNA) per output. The beamwidth can be optimized to near constant over a wideband and therefore offer very interesting solutions for radio telescopes. The quad-ridge technology allows for a significantly lower cut-off frequency for the flared out waveguides dominant mode, than the non-ridge counterpart. The combination of the ridge and horn profile allow specific properties to be tailored for the telescope. Due to the fact that these properties are very difficult to theoretically predict in terms of the profiles, it is common practice that the feed is numerically optimized to give desired performance. Several dimensions of the feed are included in this optimization, the ridge and horn profile, thickness of the ridges, distance between opposite ridges, back-short design, feeding point and flare angle. An illustration of the QRFH is shown in Figure 2.6 where the ridge and horn profiles are illustrated, the two orthogonal ports feeding the horn are illustrated in Figure 2.7.

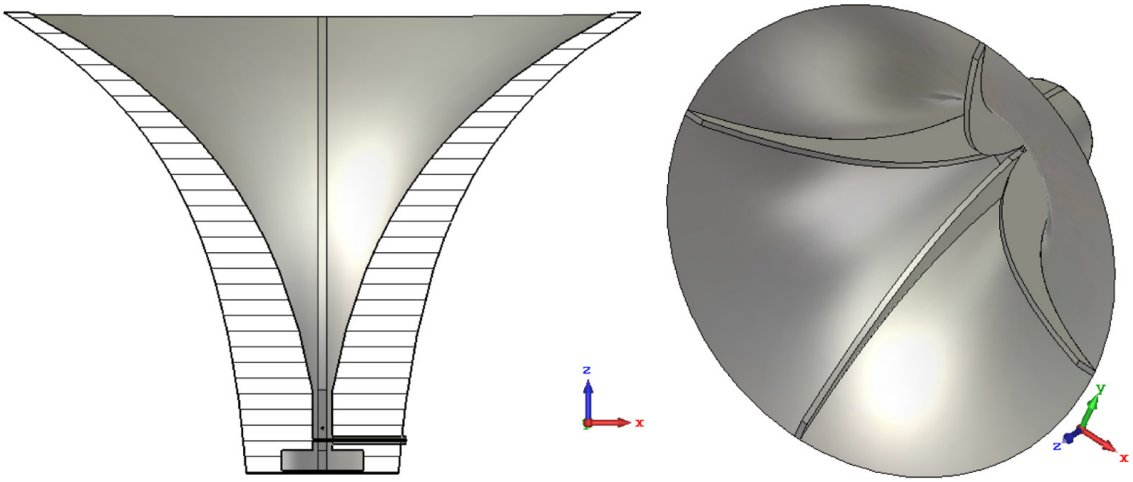

Figure 2.6: Quad-Ridge Flared Horn illustrated with a cross-section through the middle (left) and a perspective view of the opening and ridges (right).

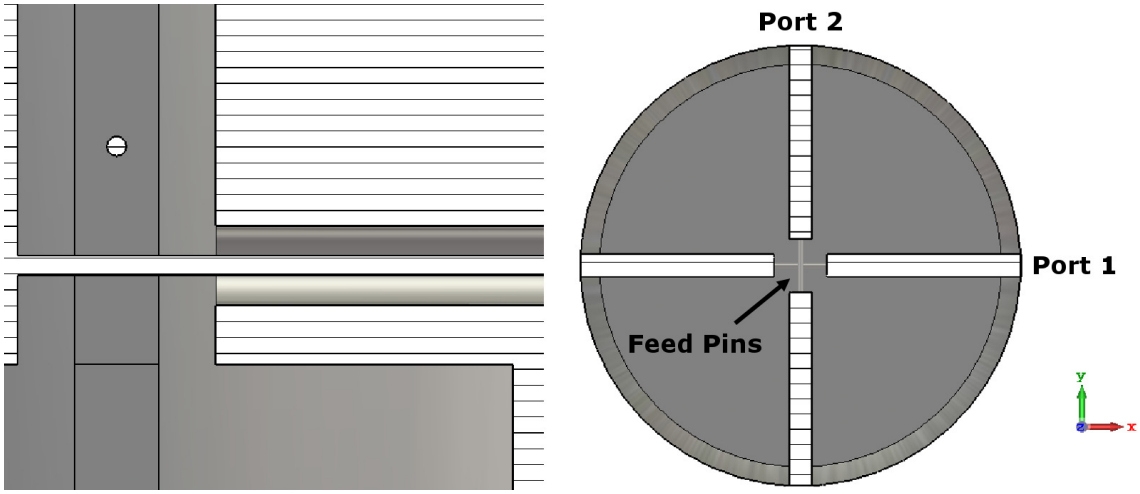

Figure 2.7: Quad-Ridge Flared Horn feeding illustrated with a cross-section through the coaxial line (left) and a cross-section above the feeding point for the two orthogonal ports (right). Feeding pin for the orthogonal polarization in the left figure is seen as a dot. In this illustration, air-coaxial lines are used.

Depending on the design, when the feed is manufactured and assembled special attention has to be put on the contact between the ridges and the horn. If the feed is molded into one big piece, this is of no concern however, if the feed is assembled from several parts (which is more realistic) this is crucial for the radiation and loss properties. The tolerances of the ridge and horn profile as well as the back-short and feeding section are very important. For lower frequencies, e.g. $350 - 1050$ MHz, these dimensions are bigger than the tolerance levels of manufacturing, which makes it less crucial in this case.

2.5.1 S-parameters

This property is not QRFH specific, but is explained here in the simplest and most relevant way to the project. S-parameters generally relates the input and the output of a system. For a two-port system, like the QRFH, S_{11} and S_{22} is the complex reflection coefficient for port 1 resp. port 2. In the case of a feed antenna that radiates, the coefficient S_{21} represents the coupling from port 1 to port 2. S_{12} is the reverse of this and these should be symmetrical. The coupling should be very low between the ports. The remainder of the excitation power will be in form radiation and also a small amount of dissipative losses. Even though the QRFH is almost symmetrical the reflection coefficients for the two ports are different due to the fact that they are separated physically. Therefore, the matching is not identical, and the phase should obviously differ.

3
Specifications and Requirements

In the thesis we refer several times to specifications and requirements we aimed for during the project, this sections will state these in an as short and clear way as possible. What goes into these requirements will not be discussed in this thesis as it is outside the scope. It is important to note that these specifications are only fully relevant for the full-scale feed results discussed in Section 5.2.

3.1 SKA Dish

The offset Gregorian dish geometry mainly used in this thesis, is designed for an effective projected diameter $D_p = 15$ m, according to definition in Figure 2.3. The MR measures 15 m in width and above 18 m in length and the SR diameter is above 5 m, dimensions are illustrated in Figure 3.1. An extension of the SR shape is included on the lower side (closest to ground) which reduces the ground noise pickup, see Figure 2.3. The dish has a half-subtended angle of $\theta_e = 58°$ and is defined according to Figure 2.4. We will refer to this dish geometry in the text as the *SKA dish*.

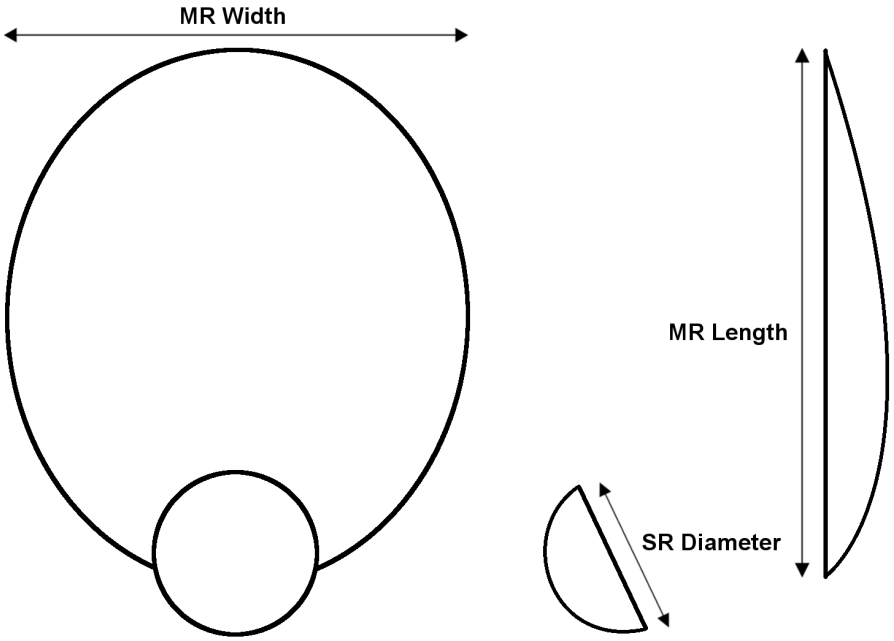

Figure 3.1: Illustration of dimensions for an offset Gregorian dual reflector geometry. (Left) Front view, (Right) Side view.

3.2 Bandwidth

The specified frequency band is $350 - 1050$ MHz and according to Equation 2.6 corresponds to a fractional bandwidth of

$$B = \frac{1050}{350} = 3 \rightarrow 3:1. \tag{3.1}$$

3.3 S-parameters

Reflection at the feed port is desired to be as low as possible, with the requirement of $|S_{11}|, |S_{22}| < -10$ dB. The orthogonal port coupling $|S_{21}|, |S_{12}|$ must be reasonably low, in this case around -40 to -50 dB.

3.4 Aperture Efficiency

We did not specify a strict requirement for the aperture efficiency, η_a, but with a goal to reach at least 70 % across the band. This is due to the fact that an absolute constraint here, could limit the performance in sensitivity due to the mentioned trade-off with spill-over.

3.5 Sensitivity

This is the most important specifications in this thesis and the figure of merit for the system. A_{eff}/T_{sys} shall increase from at least 2.1 m^2/K at 350 MHz to at least 4.2 m^2/K at 650 MHz and from there it shall stay above at least 4.2 m^2/K up to 1050 MHz. We also have the requirement of an average across the band of at least 4.2 m^2/K. These levels must be fulfilled down to $|\theta_p| = 60°$.

3.6 Intrinsic Cross-Polarization

The intrinsic cross-polarization (IXR) minimum must be above 15 dB across the band.

3.7 Far-out Side-lobes

We require that side-lobes outside $\theta = \pm 10°$ or the 8^{th} null for all ϕ across the frequency band, is below 6 dBi. As the frequency increases, the beam will get narrower and $\theta = \pm 10°$ will be outside the 8^{th} null. The second condition on the far-out side-lobes, is that the total solid angle of side-lobes above 0 dBi outside $\theta = \pm 10°$ cannot be larger than 0.05 steradians (sr).

4

Design Methods and Analysis Tools

The methods for the feed development have been evaluated and modified continuously during this work. The reference evaluation tool for the feed design is the complete system simulator [12] that emulates the telescope performance on sky with a realistic noise model. We started the design phase with tailoring the stochastic optimization algorithm in the feed optimizer [11] for accurate and quick simulations. Both of these simulation tools was provided by Prof. Marianna Ivashina in the Antenna Group, Signals and Systems department at Chalmers University of Technology. We also implement a spline QRFH model, where the initial model was provided by Dr. Isak Theron and Dr. Robert Lehmensiek at EMSS Antennas [8] in South Africa, that parametrizes the entire horn design to allow for separate optimization of individual parts. Apart from these design tools work was done by individual design and optimization in CST, and to some degree MATLAB, to achieve the desired specifications for the feed system. During the entire process, control simulations were run in FEKO through both physical optics (PO) and full-wave analysis for confirmation of the results. Furthermore, at certain milestones during the project the feed model performance was confirmed through simulations by Dr. Robert Lehmensiek with an independent system model.

4.1 Spline QRFH Model

During previous work for developing a QRFH feed for Band 1 several ways of modeling the horn and ridge profile were evaluated. Modeling the horn and ridge flare with an exponential function is a way to create a smooth and mathematically well defined profile [9]. However, during optimization we concluded the spline profile to be advantageous in finding a trade-off between aperture efficiency and minimization of spill-over noise, over the $3:1$ bandwidth (paper A.1). The concept of the spline model is based on the outer profile of the horn and the inner profile of the ridge being parametrized with a set of point coordinates. The points are individually optimized through an algorithm and for each iteration they are combined together with the intrinsic CST spline-function to smooth profile curves, illustrated in Figure 4.1(a). The outer curve profile is then rotated around the boresight axis to form the shape of the horn and together with the inner curve constructs the ridge profile, illustrated in Figure 4.1(b). The other parts included in the feed such as the ground plane, feeding point, back-short and ridge thickness etc. are also parametrized for

optimization.

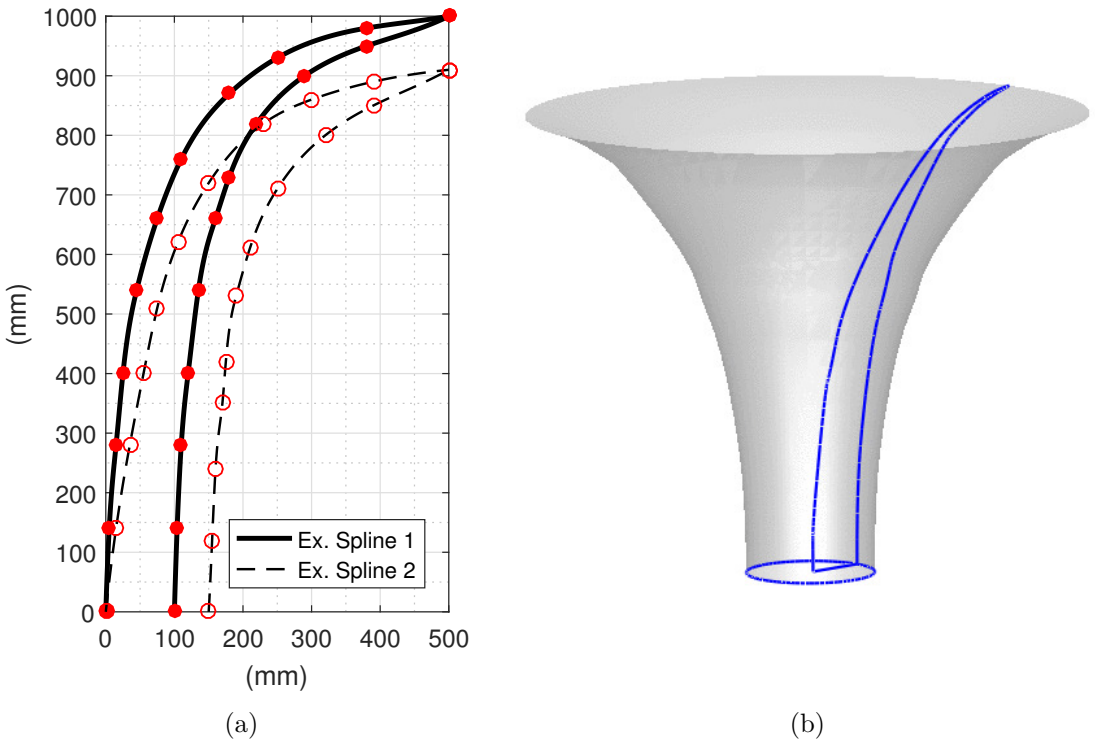

(a) (b)

Figure 4.1: The horn and ridge spline profile concept is illustrated here. (a) Examples of two different profiles for the ridge and horn (horn profile is the right-most curve for resp. example spline), where the dots represent the x- and y-coordinates of the spline points. (b) Example of a ridge spline profile and a horn spline profile swept 360° to form the horn shape.

4.2 Feed Optimizer

The optimization software [11] uses CST which implements a version of finite-difference time-domain method (FDTD) solver for accurate electromagnetic simulation of the feed design. These results are then passed through a physical optics and diffraction solver in GRASP to simulate the performance on the dish. This result is then evaluated in the full system level analyzer for accurate sensitivity and noise analysis from the given noise model (see Section 4.3). The entire process is controlled and implemented through MATLAB and optimized with an evolutionary stochastic algorithm, see full optimization schematic in Figure 4.2. Tailoring the feed to a specific dish geometry through multiple iterations in combination with the parametrized spline model of the feed, gives a highly optimized design. Several different setups were used during optimization: large parametric search space (large number of parameters to optimize); parametric search space divided into different parts; larger optimization runs (many iterations); small runs with fine tuning as the goal. The choice of optimization algorithm is dependent on the parameter search

space and the goal of each optimization run and the two most important algorithms are explained in Sections 4.2.2 – 4.2.3.

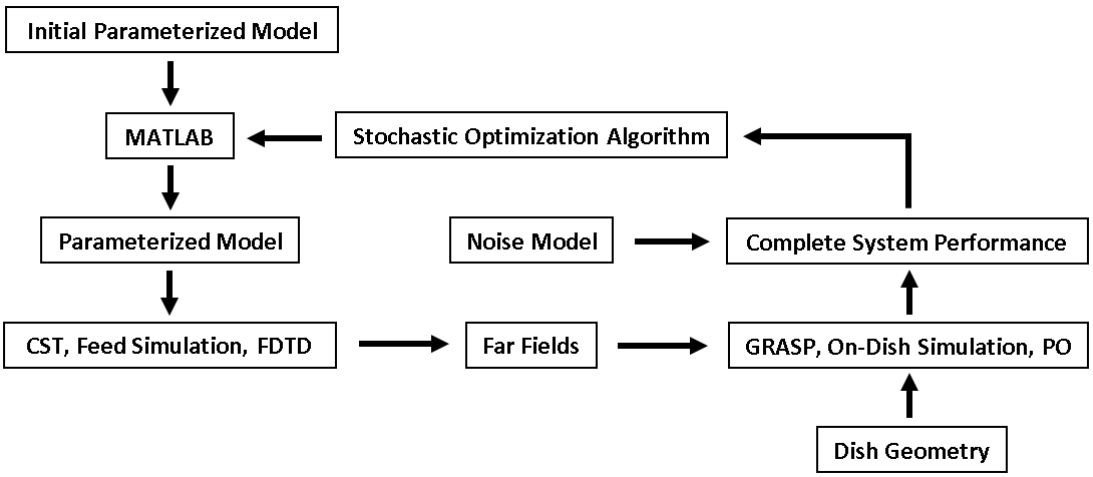

Figure 4.2: Schematic overview of the feed optimizer process where one complete loop corresponds to one iteration.

4.2.1 Fitness

In stochastic optimization the fitness number of each iteration evaluates how the model is improving. The performance is evaluated according to specifications and specific weight is assigned to crucial properties of the design that is to be enhanced. As a feedback system the fitness number is fed through the algorithm which then pushes the optimization in a preferable direction. To exemplify the concept of fitness number (and fitness function) we assume a very simple system with three linear properties that should be optimized, we denote these as x_1, x_2, x_3. For the sake of understanding we assume each of these properties have different importance to the end result, hence they should be weighted differently. We denote the individual weights for each property as w_1, w_2, w_3 and the simplified fitness number, F, is given according to

$$F = w_1x_1 + w_2x_2 + w_3x_3. \tag{4.1}$$

If we assume the properties to be considered better with an increase in value, we would want F to increase in total. To indicate, for example, that property x_1 is the most important to increase, the w_1 weight should be large. This would, when x_1 is increased, give a large increase in F and therefore show that the particular change that was made in the model is beneficial for the optimization. This example model is simplified for illustration purpose and the dependencies between the different properties x_1, x_2, x_3 is not considered, this is not the case in the feed optimization. Specific weight was put on low input reflection and impedance matching, high aperture efficiency and high sensitivity for the feed optimization. As already mentioned the trade-off between aperture efficiency and sensitivity (spill-over noise) is quite important to account for in the fitness function. Weighting either of these

properties inappropriately could drive the algorithm into a local extremum and halt the improvement of the optimization run. Therefore, specific effort were put into tuning the fitness function for each optimization setup.

4.2.2 Particle Swarm Optimization

In stochastic optimization [27] the particle swarm optimization (PSO) [28] is a very powerful concept for investigating a large search space. PSO is similar to other evolutionary algorithms in the sense that it uses a population of potential solutions across the parameter search space. These solutions, or *particles*, have well known *position* and *velocity* (Heisenberg would not be happy) and are aware of their own local best solution. Furthermore, they all share knowledge of the best global solution which draws the group of particles, or *swarm*, towards what could potentially be an advantageous area to find the global extremum, if there is one. Since the current best positions, both local and global, are constantly updated the particle swarm can in a fast way cover very large search spaces with less computational power. The initial positions and velocities of the particles are a key setting for a successful optimization run. Setting a too large number of particles in the swarm could potentially lead to unreasonably long computational time. If the number of particles or initial velocities of the particles are too low, the swarm could end up in a local extremum.

4.2.3 Genetic Algorithm

Genetic algorithms (GA) are a standard approach in stochastic optimization and have many similarities with PSO, however the definition and optimization setup is different. The GA is based on the natural selection principle which utilizes both random and selective evolution to find the best solution of the optimization object. Initially the algorithm starts with a population set, a set of *gene* (parameter) combinations, which is evaluated with a fitness function that feeds back how well adjusted the solution is to the algorithm. The populations are then evolved through selections that are transferred to the next generation. This selection could happen both through a random and selective approach, since only transferring the ”advantageous” genes could send the algorithm to a local extremum. The populations selected for evolution are then combined through different methods, for example *cross-over* where two or more population genes are combined or *mutation* where genes are randomly changed. Probability and combination settings for the methods of evolution is important to the success of the algorithm. For fine tuning an initially good population, for example a promising feed model, the GA is an excellent choice since the possibilities of tailoring the algorithm are many and a narrow search space could be defined and investigated effectively.

4.3 System Simulator

The core of the feed optimizer and the full system analysis of the enhanced feed design, is the MATLAB-based system simulator [12]. In the lower right part of Figure 4.2 a simplified schematic of the basic process is shown. With a full dish

physical optics simulation from GRASP the system simulator evaluates the beam patterns and calculates aperture efficiency, sensitivity and cross-polarization levels etc. As emphasized in Sections 2.4 – 2.4.1 the calculation of spill-over noise pickup in the total system noise is important for the feed optimization and is one of the key features of the system simulator. To calculate the spill-over noise and antenna noise temperature according to Equation 2.25, a model of the surrounding noise temperature is implemented. This model assumes a constant ground noise temperature, T_g, for the lower half-sphere and a zenith angle (θ_p), azimuth (ϕ) and frequency (f) dependent noise temperature, $T_s(\theta_p, \phi, f)$ of the sky on the upper half-sphere, illustrated in Figure 2.5. Other contributions from the feed, back-end and LNAs' are included in the system analysis of sensitivity as frequency dependent quantities. As mentioned, this detailed calculation of the feed performance on the dish, allows for a very specific tailoring of the feed optimization to fulfil the system requirements.

5
Results

In this section simulation and measurement results from different stages of the feed design process will be presented. Antenna characteristics such as S-parameters, beam patterns and efficiencies shows the development from early optimization phase and scaled prototype design to the full-scale feed design that has been prototyped. The sections concerning full-scale Band 1 prototype called the "Sep2015" will focus on the resulting performance of the optimization procedure, whilst the scaled Band 1 design will detail the process of optimization. The process is of course very similar, but the performance of the full-scale model are more interesting as it is part of the main goal of this thesis.

5.1 OQRFH Band 1 Scaled, $1.5 - 4.5$ GHz

To ensure a valid approach of the feed optimization process and ensure early prototype confirmation of the antenna characteristics a scaled QRFH was simulated and manufactured. This design was scaled and modified to operate in the frequency range $1.5-4.5$ GHz. This project was intended as a learning exercise on how to setup a large optimization for the full-scale horn and get acquainted with the optimization software and at the same time prove the technology readiness for prototyping a feed design. We aimed for aperture efficiency to be $\eta_a > 70$ % across the band, and a level of sensitivity $A_{eff}/T_{sys} \geq 4$ m^2/K, assuming a constant $T_{REC} = 10$ K. The reflector geometry for this process is, just as the SKA dish, an offset Gregorian but with a smaller SR, a smaller MR with $D_p = 13.5$ m and a half subtended angle below 50°. This means that when the feed is simulated on the bigger SKA dish, the performance will be different.

5.1.1 Optimization

The technique of PSO, explained in Section 4.2.2, was implemented for the feed optimization due to the large parameter space. The complete model consists of 42 parameters to build the shape of the feed. More than half of these parameters constitute the x- and y-coordinates for the points in the spline profiles of the horn and ridges (see Section 4.1). At this time in the optimization process, the GRASP-evaluation time for frequencies in Band 1 ($350 - 1050$ MHz) was quite fast which would supply a large number of iterations in a reasonable amount of time. However, the scaled Band 1 frequencies of $1.5 - 4.5$ GHz gives, with the *adaptive* reflector meshing in GRASP, a finer grid and therefore simulation time is increased. With

0.25 GHz step (13 frequency points) one iteration consumes about 1.5 hours, where the CST simulation of the feed itself would take approximately 10 minutes of this time. This would prove to be too time consuming to achieve reasonable convergence with the size of the parameter space. In the evaluation of the feed performance, 13 frequency points is already a too low number to give representable evaluation of the entire band. However, since this part of the project was to prove the process of optimization, a trade-off was made to go even lower in frequency resolution with a 0.5 GHz step. The time for full convergence of the algorithm for such a large parameter space still proved to be too long for the purpose of this exercise. Therefore, in an attempt to get some fast improvements, the process was divided into optimization runs of different parts of the horn particularly the ridge profile and the horn profile optimized separately. Due to time constraint and the partial goal of this project to show technology readiness, a decision was made to use an early proven version of the feed (similar to the scaled original feed) for the prototype manufacturing. This design and its performance is documented in Sections 5.1.2 – 5.1.4. In parallel, the optimization process continued and in Figure 5.1 an illustration of convergence can be seen for optimization only focusing on the ridge profile and its thickness. The PSO algorithm was here searching for a minimum point and therefore the improved model has a lower fitness number. It can also be seen here that after 200 iterations the algorithm is saturated in terms of the fitness improving for this setup.

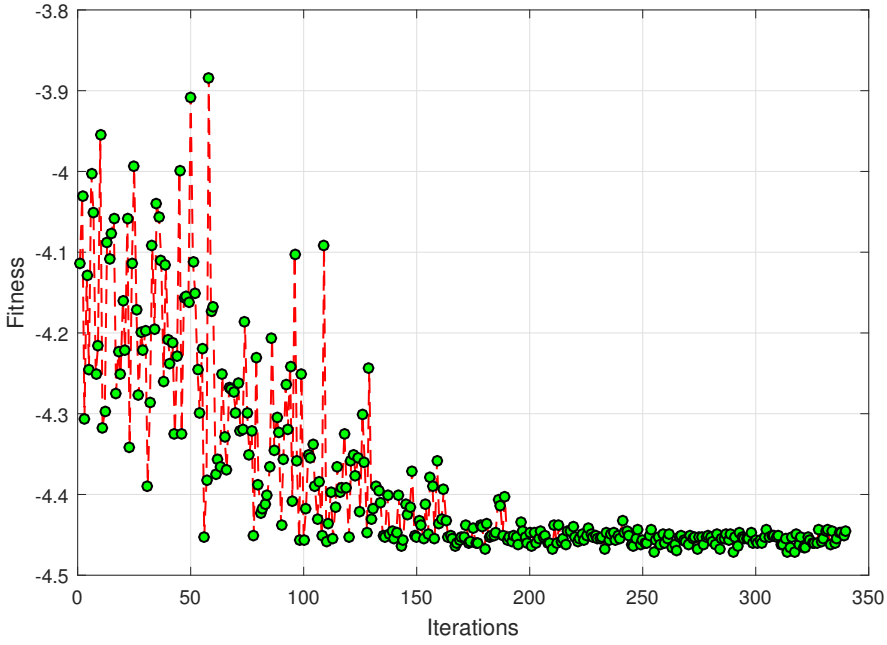

Figure 5.1: Illustration of the convergence of an optimization run focusing on the ridge profile for the scaled Band 1 feed. The fitness function of the algorithm focused on improving the sensitivity of the model.

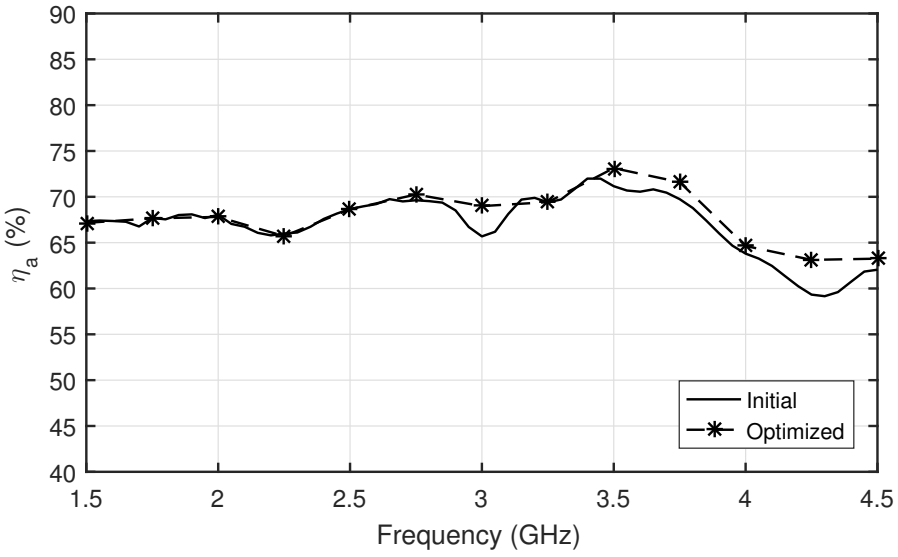

(a)

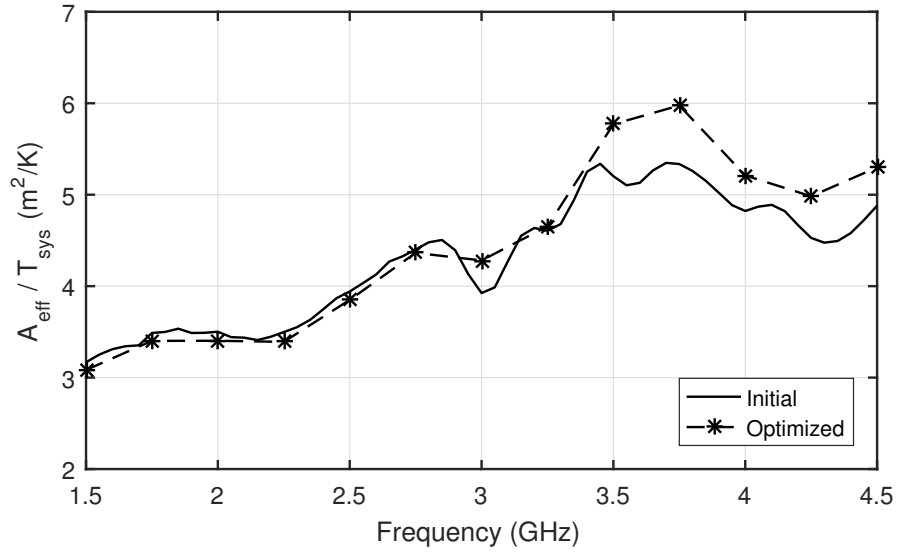

(b)

Figure 5.2: Scaled Band 1 feed design initial model compared to an optimized version. (a) Aperture Efficiency. (b) Sensitivity, assuming constant $T_{REC} = 10$ K. Note that the number of frequency points in the curves are different.

In Figure 5.2 the aperture efficiency and sensitivity of an optimized model (best fitness value) is compared to the initial. There is a clear improvement at the higher frequencies in sensitivity which proves the value of the optimization technique. This result looks promising, however there are aspects regarding the coarse frequency resolution that needs to be accounted for. The resolution during optimization of the model was only seven frequency points per iteration (Figure 5.2 displays 13 frequency points). The improvement at 3 GHz of about 3% in aperture efficiency, could simply be a shift of the ”dip” to nearby parts of the band that is not uncovered

with such a low frequency resolution. Similarly, the clear improvement at higher frequencies could also be caused by this type of hidden results. We conclude that a finer frequency resolution is preferred, to not mislead the optimization routine in the wrong direction, perhaps to a local minimum where parts of the band has been improved by "secretly" sacrificing other parts. This was an important reason, due to time constraints, why a proven model was chosen for prototyping early during the project. During the course of this project there were other similar optimization runs. Different variations of the algorithm and the fitness function setup was investigated. However, since the prototyping had started and the main goal was an optimized full-scale feed design, no more results from scaled Band 1 feed optimization will be shown here, only the performance of the manufactured prototype.

5.1.2 Electromagnetic Design

From here on the dish used in the simulations will be what we call the SKA dish, therefore results will be different from the previous shown. The goal of Section 5.1.4 is to show that the simulated performance of the scaled Band 1 feed matches the measured performance reasonably well. Feed dimensions measures roughly 24 cm in height and similar in diameter. The ridges are excited with two coaxial feed lines, one for each polarization (opposite pair of ridges) separated by 90°, see Figure 2.7.

5.1.3 Mechanical Design

The transition from an electromagnetic model in CST to a mechanical CAD-design is not trivial. Despite this, it was done impressively fast by the Electronics Laboratory group and Mechanical Workshop at Onsala Space Observatory in a very limited time frame and with great results. Many things need to be considered in this process such as manufacturing technique, how to assemble the parts, tolerances and materials. This is outside the scope of this thesis and will therefore not be assessed in detail. There are some intentional differences in the mechanical CAD-model compared to the electromagnetic model, see Figure 5.3. The body of the horn is mechanically lathed from a solid piece of aluminum and therefore we have added material around the horn, so that it is more easily clamped in the machine. It is also preferred when considering the assembly of the ridges and feeding that are screwed in to the horn. To ensure a good enough contact between these parts, as many screws as possible are desired (within reason). The ground plane of the feed is completely parallel to the horizontal plane. This was specified to make the contacting easier in the mechanical prototype, and make manufacturing easier. The inner shape of the horn and the ridge-profile must be kept strictly the way they were designed, as this is a crucial part for its electromagnetic performance, emphasized in Section 2.5. The ridges were machined very accurately in-house at the observatory mechanical workshop.

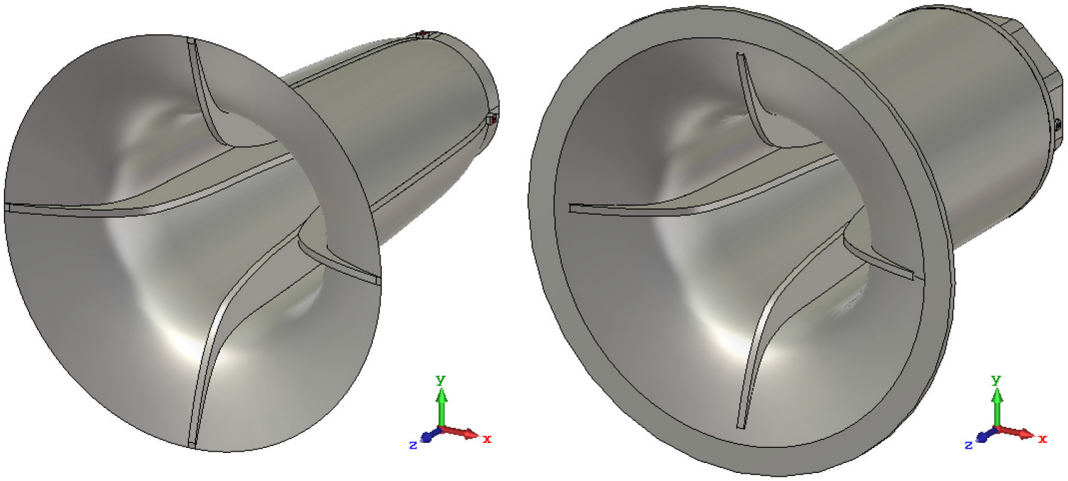

Figure 5.3: The scaled Band 1 prototype design in perspective view. Left: Electromagnetic Model; Right: Mechanical Model.

Before final decision was made to start the prototype manufacturing, we compared simulated results for the electromagnetic model and the mechanical CAD-model. This was done to ensure that the electromagnetic performance was consistent in the detailed mechanical model and that no unintentional design altercations had occurred. Figures 5.4 – 5.5 show this result comparison of the feed alone and simulated on dish. From the beam patterns in Figure 5.4 we can see that the overlap is not complete, only horizontal polarization (port 2) is plotted for convenience. This is expected as the ridge flare and aperture of the mechanical model is slightly different from the original design which alters the radiation properties. The ridge is made with a slightly different thickness than initial design, to better match available materials. However, in Figure 5.5 the performance on dish is confirmed and the small deviations in the beam patterns do not affect the overall performance.

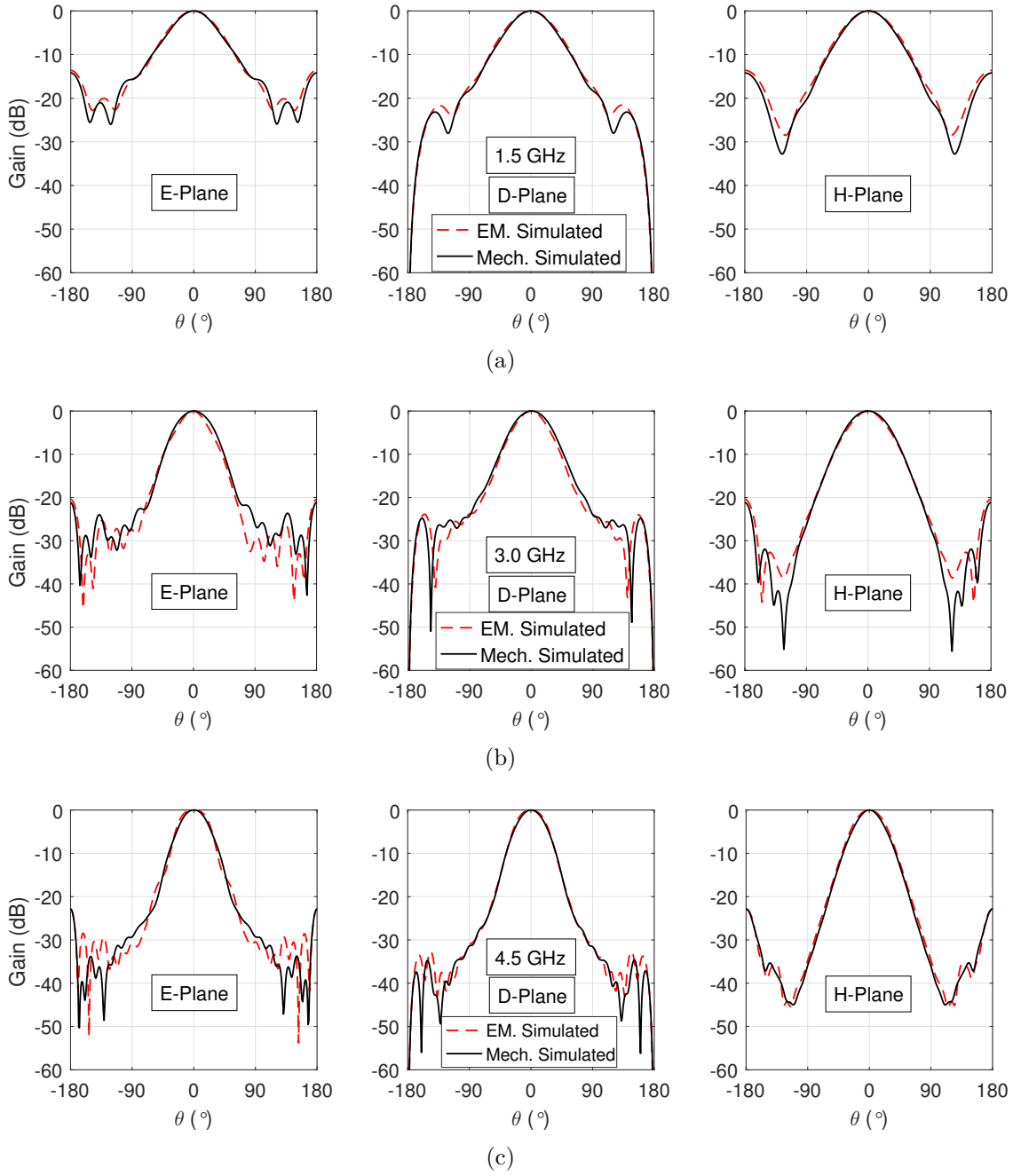

Figure 5.4: Simulated beam patterns for the scaled Band 1 for electromagnetic (EM) and mechanical (Mech) design in (left) E-, (middle) D- and (right) H-Plane. Solid black represents horizontal polarization (port 2) of the mechanical model and the dashed red curve represents horizontal polarization of the electromagnetic model. (a) 1.5 GHz. (b) 3.0 GHz. (c) 4.5 GHz.

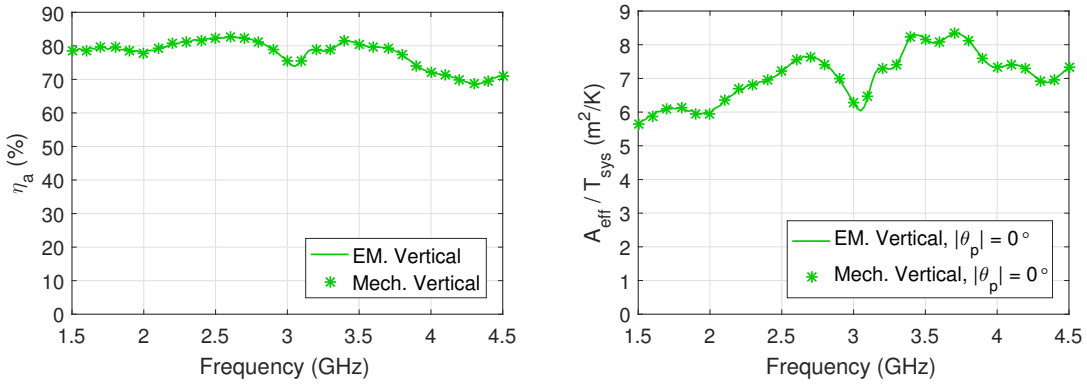

(a) (b)

Figure 5.5: Confirmation simulations of the scaled Band 1 feed electromagnetic and mechanical model on the SKA dish. (a) Aperture Efficiency. (b) Sensitivity, $T_{REC} = 10$ K.

5.1.4 Prototype and Measurement

In Figure 5.6 the assembled prototype is shown, note the excitation pins for the two polarizations crossing each other in bottom of the feed. On the side of the feed, the screw holes following along the profile can be seen. As discussed earlier, it is important to ensure a good contact between the horn and the ridges and enforcing the alignment to the opposite ridge. The holes are placed as close as possible without jeopardizing the material structure.

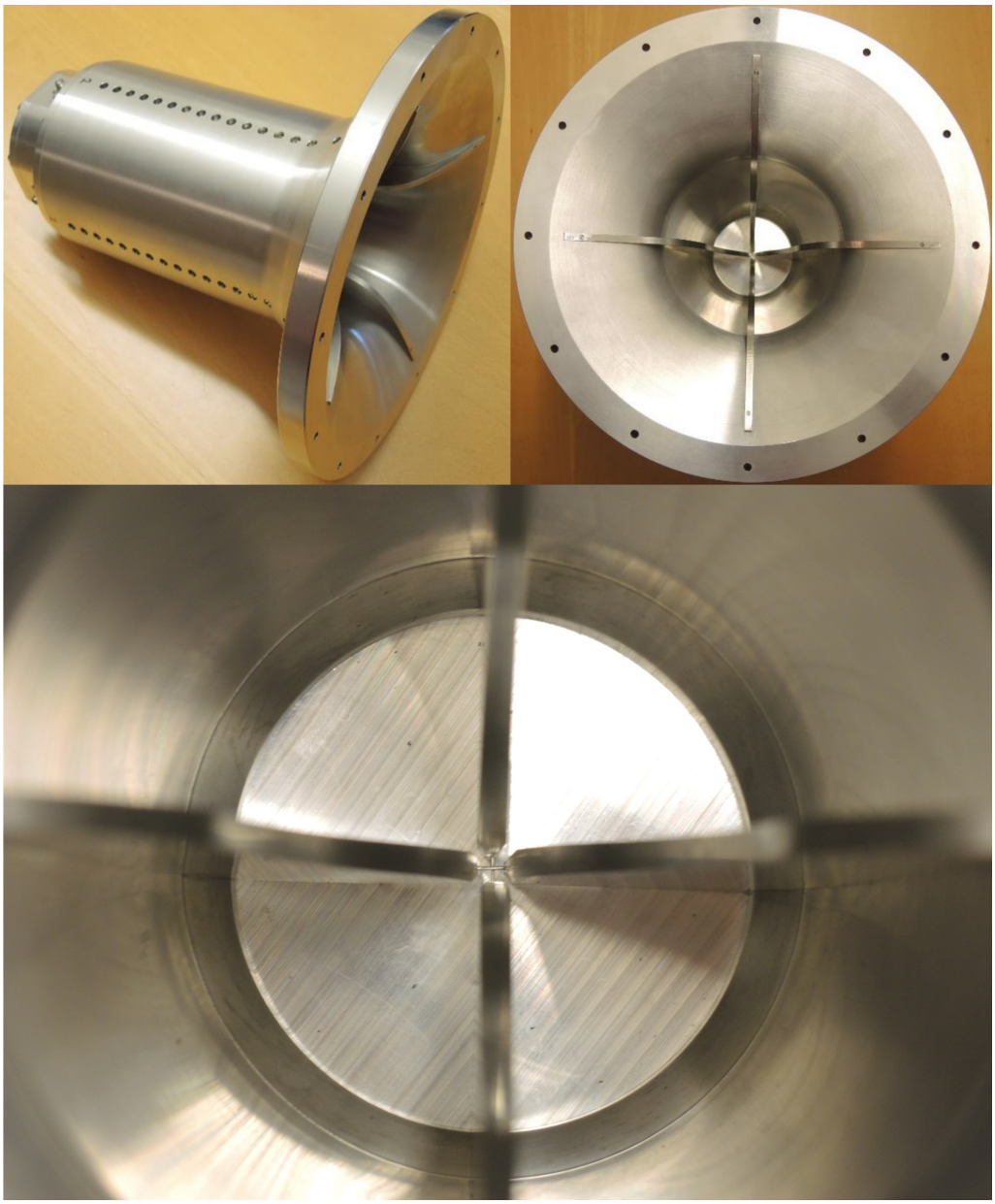

Figure 5.6: Scaled Band 1 feed prototype assembled. Top left and top right shows the complete feed, bottom shows a zoomed in view of the coaxial excitation pins.

5.1.4.1 S-parameters

The reflection and coupling coefficients of the prototype was measured at Onsala with a network analyzer (Agilent Technologies E83262C). During measurements the unused port was terminated with a 50 Ω load. In Figure 5.7 the simulated and measured reflection coefficient for each port shows good agreement. The small deviations, specially at higher frequencies, can partly be related to the mesh resolution of the simulations, but most likely some small physical deviations in the manufactured prototype. The coupling coefficient is simulated to be lower than −50 dB and therefore very hard to measure accurately, however the measured level does not show any implications of too high coupling between the ports.

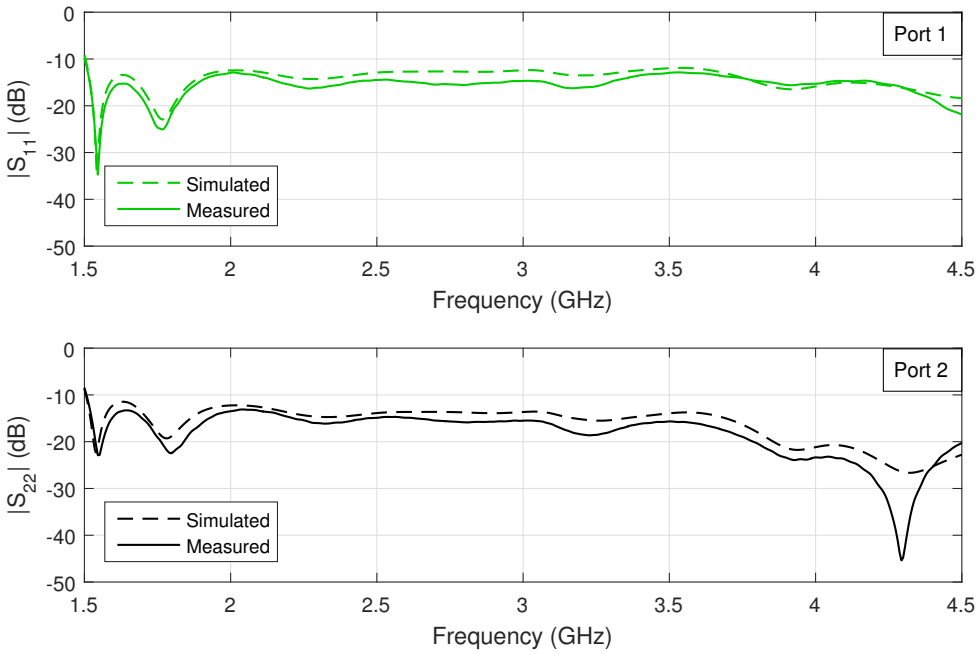

Figure 5.7: Simulated and measured input reflection coefficients for the scaled Band 1 feed prototype both vertical polarization (top, port 1) and horizontal polarization (bottom, port 2).

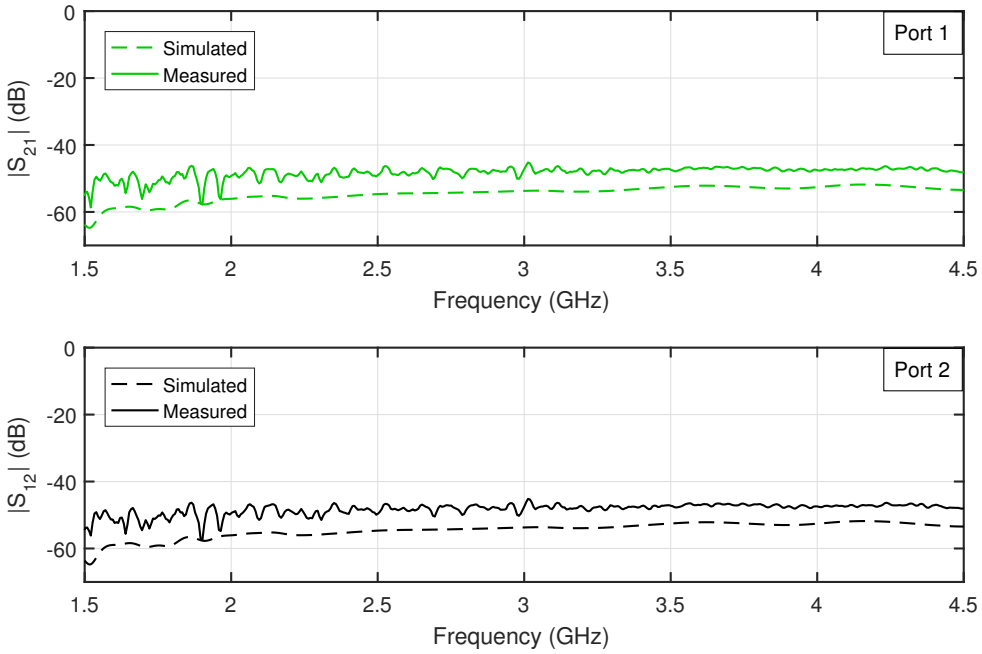

Figure 5.8: Simulated and measured coupling coefficients for the scaled Band 1 feed prototype both vertical polarization (top, port 1, coupling to port 2) and horizontal polarization (bottom, port 2, coupling to port 1).

5.1.4.2 Beam Patterns

The radiation performance of the manufactured feed prototype was measured at Sigma AB in Lund, Sweden in a Satimo S64 anechoic chamber. The feed was placed on a rotating pedestal under an arch containing 64 reference antennas, see Figure 5.9, which made it possible to get the complete beam patterns for the feed in all directions of the sphere. In Figure 5.10 we compare beam patterns for three frequencies at different ϕ. The dynamic range of the measurement station probably affects the results here, and unwanted reflections may have contributed to the back-lobes. Deviations in the manufactured parts, i.e. misalignment and tolerances, is of course a factor here as well. However, the normalized beam patterns show good agreement with the simulated results. It was concluded that the accuracy of the test range was not good enough to measure the total radiation efficiency in a sufficient way.

Figure 5.9: Scaled Band 1 feed prototype in the anechoic measurement chamber, the yellow crosses are the reference antennas that span the arch around the feed. Walls are covered in absorbing material to minimize unwanted reflections.

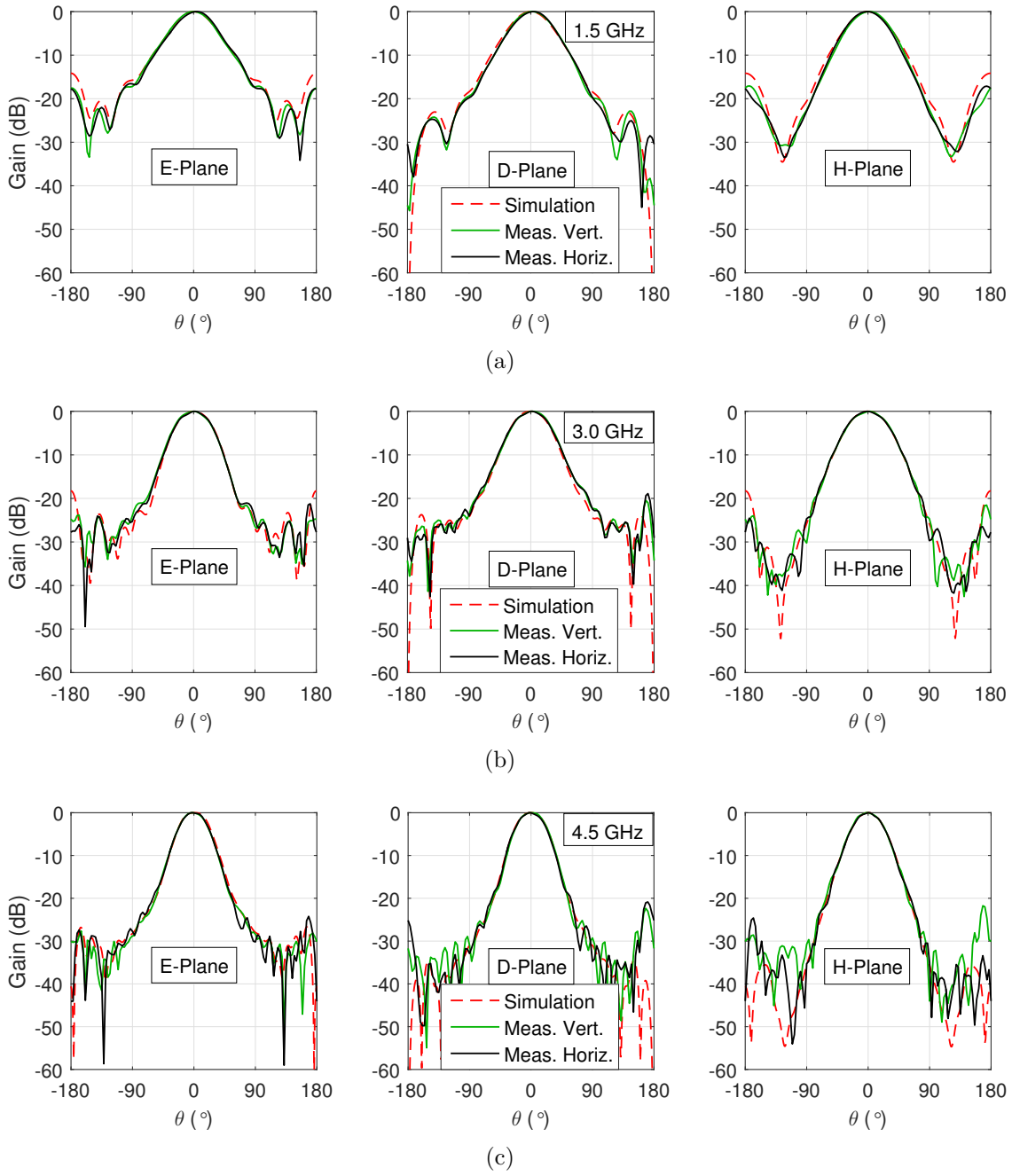

Figure 5.10: Simulated and measured beam patterns for the scaled Band 1 feed in (left) E-, (middle) D- and (right) H-Plane. Solid green represents measured vertical polarization (port 1) and solid black represents measured horizontal polarization (port 2) with the dashed red curve representing simulated results. (a) 1.5 GHz. (b) 3.0 GHz. (c) 4.5 GHz.

5.1.4.3 Aperture Efficiency

A comparison of η_a between simulated and measured beam patterns evaluated on the SKA dish can be seen in Figure 5.11. The agreement is reasonable and the deviation, specifically at the high end of the band, is related to the uncertainty of

the measured beam patterns and the phase center location relative the dish focal point. Despite the phase centers of all frequencies should be close to the same, this can affect the illumination of the dish.

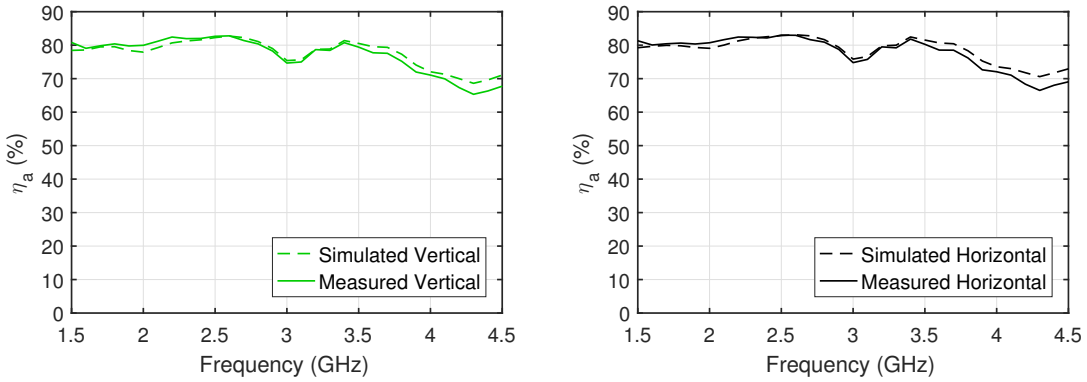

(a) (b)

Figure 5.11: Simulated and measured aperture efficiency, η_a, for scaled Band 1 feed on the SKA dish (a) Vert. pol. (b) Horiz. pol. Dashed curves are simulated, solid curves are measured. Resolution: 0.1 GHz.

5.1.4.4 Sensitivity

The deviation in the aperture efficiency (Figure 5.11), translates into a drop in A_{eff}/T_{sys}, see Figure 5.12. Furthermore, the side-lobe levels measured in Figure 5.10 at high frequency can also contribute to an increased spill-over noise pickup and therefore a degraded sensitivity. Receiver noise is here assumed to be a constant $T_{REC} = 10$ K, for comparison only. The agreement is acceptable under these conditions and generally confirms the expected result for this prototype.

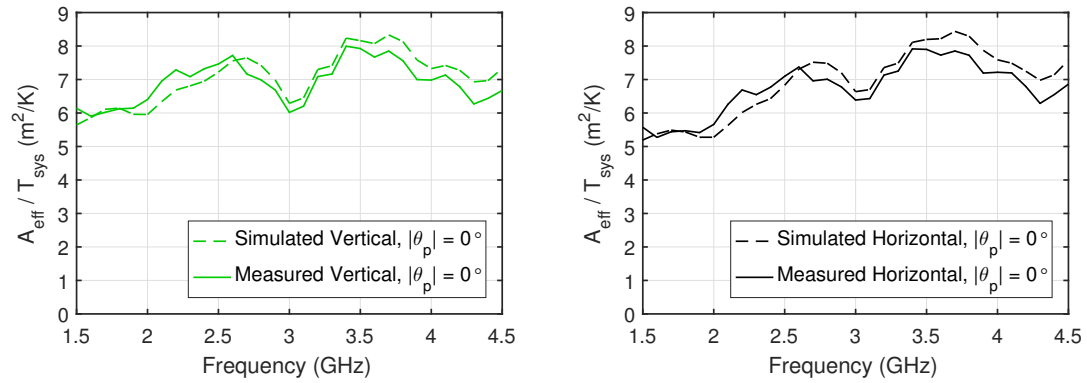

(a) (b)

Figure 5.12: Simulated and measured sensitivity, A_{eff}/T_{sys}, for scaled Band 1 feed on the SKA dish with $T_{REC} = 10$ K. (a) Vert. pol. (b) Horiz. pol. Dashed curves are simulated, solid curves are measured. Resolution: 0.1 GHz.

5.2 OQRFH Band 1 Sep2015, $350 - 1050$ MHz

The feed design for SKA Band 1 frequencies is destined for a large physical size due to relatively large wavelengths of $\lambda \approx 0.30 - 0.85$ m. The Sep2015 design measures about 1 m in length and with an aperture diameter of a similar size. The shape of the horn resembles that of an hourglass, unlike the more conventional funnel-like constantly increasing profile you would expect, see Figure 5.13. The special shape helps suppress unwanted modes that we experienced in the early design phase when the shape was strictly increasing in diameter. It can be seen similar to having a classic mode suppressor in the bottom part of the horn consisting of a ring around the circular shape that prevents higher-order modes. The custom shape combined with the size of the feed enables high consistent performance across the $3:1$ bandwidth without entering into cut-off at the lower side.

The feeding pins for the excitation of the ridges have been modeled by coaxial lines for the majority of the simulations. This means that the reference plane for the excitations, represented by a waveguide port, is located at the respective port marking in Figure 2.7. Reference ground plane for each pin is terminated at the opposing ridge surface. This surface plane has shown to be important for the impedance matching of the S-parameters, as has the location of the feeding points along the propagation direction of the feed. If the termination is located a significant distance inside the ridge, unexpected degradation of the reflection could occur and this is therefore important when the design is transferred to a mechanical prototype.

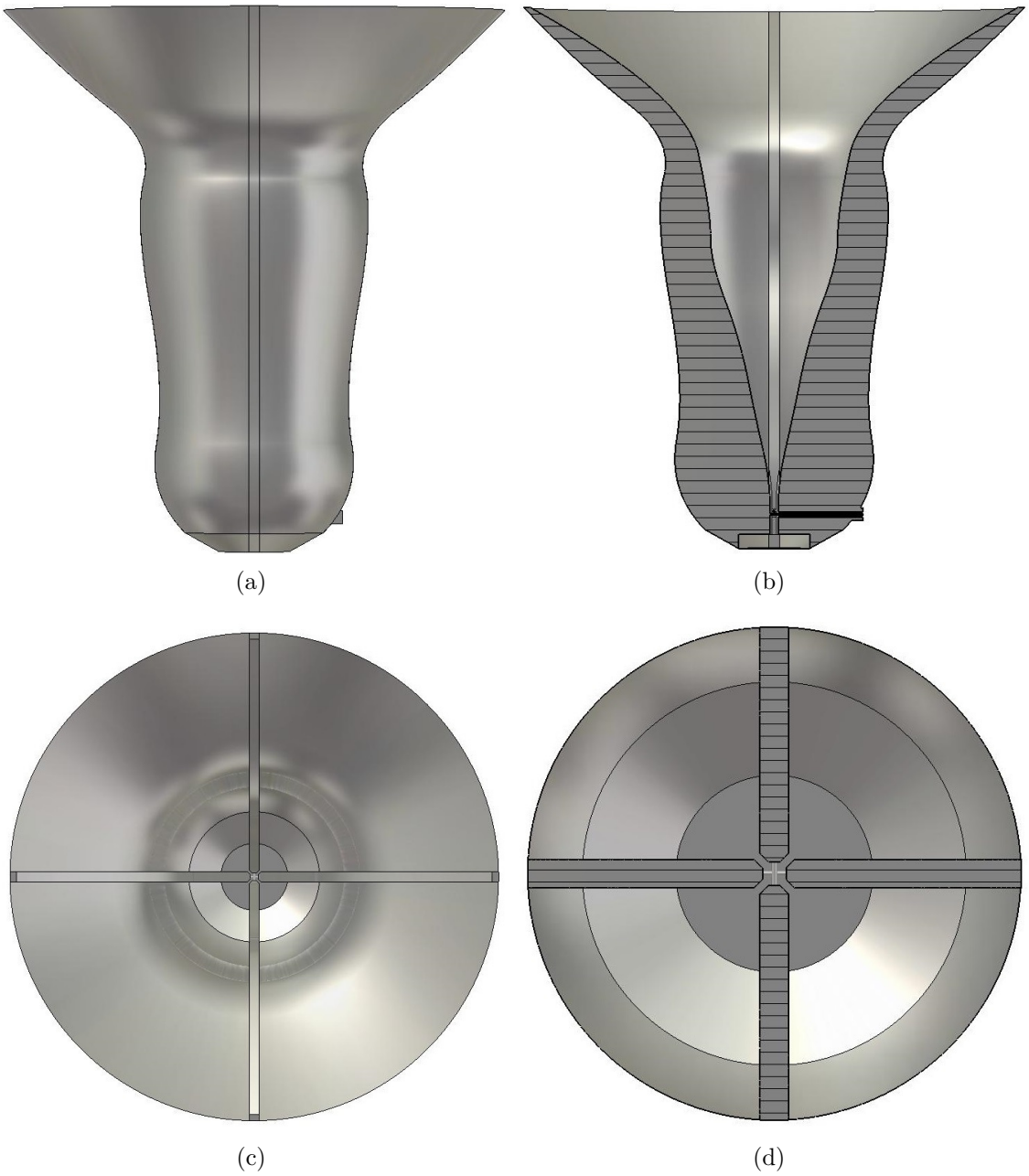

Figure 5.13: Illustrations of the Sep2015 feed design. (a) Side View. (b) Side View Cross Section. (c) Top View. (d) Top View Cross Section.

5.2.1 Optimization

Similar to the optimization for the scaled prototype, this design was optimized with PSO for the initial phase when the parameter search space was large. As mentioned we would like to use as fine grid as possible in the frequency, to resolve trapped modes at certain frequencies and show a smooth performance across the bandwidth. With a trade-off between time and frequency resolution, the fitness number for a month of iterations are shown in Figure 5.14. A decreasing fitness number means that the optimization is improving since the algorithm is searching

for a minimum. The setup for the particular run shown in Figure 5.14, included 10 frequency points across the band and the search space involved 34 out of the 42 parameters that creates the feed model. This process later resulted in the Sep2015 design after further optimization of the partial results shown here, where smaller search spaces and more frequency points was implemented to achieve convergence.

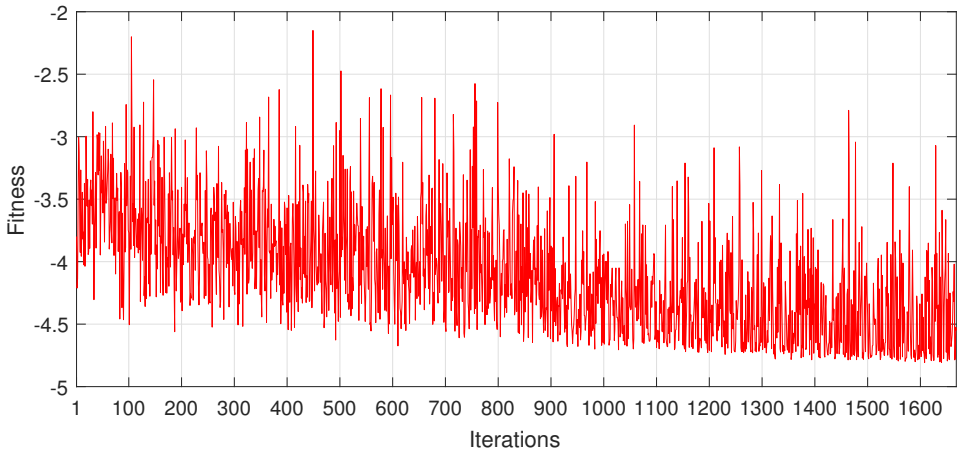

Figure 5.14: Example of fitness number progress over one month of iterations.

5.2.2 Mechanical Design

The transition from the electromagnetic model, designed in CST and used during the development stage, to the detailed mechanical design of the Sep2015 design that was prototyped, was a challenging step. This was done by the team at OSO in an impressive way with good agreement in performance between the EM and mechanical model. In Figure 5.15 we can see the high level of details for the mechanical design (right) down to the last screw. We will not detail the features of the mechanical design in the report. To exemplify the agreement in performance we see the S-parameters in Figure 5.16 for the electromagnetic model and the mechanical model ready for prototyping.

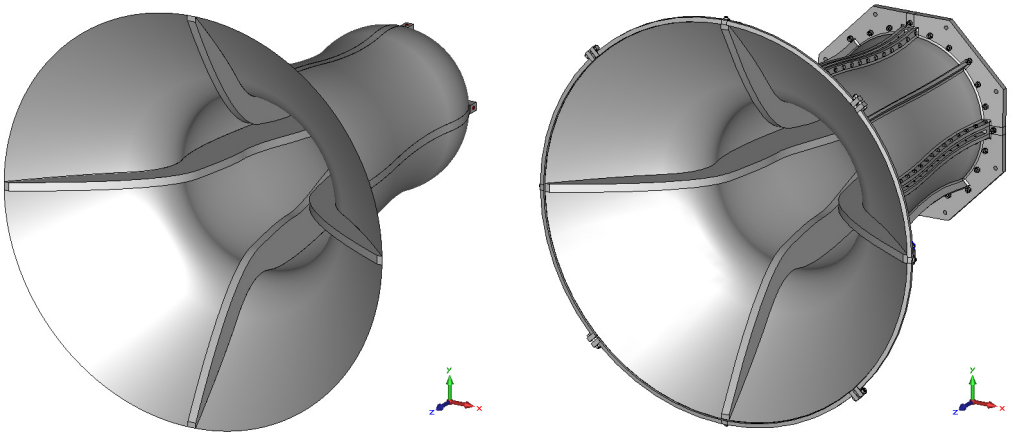

Figure 5.15: Sep2015 feed design. (Left) EM model, (Right) Mechanical model.

5.2.3 Feed Performance

In Sections 5.2.3.1 – 5.2.3.2 we show the simulated feed performance.

5.2.3.1 S-parameters

During optimization a strict constraint was implemented for the reflection coefficient $|S_{11}| < -10$ dB (of course equally strict for port 2, $|S_{22}| < -10$ dB). The matching was a challenge to accomplish in combination with the cut-off at the lower end. When scaling the feed it was also clearly seen to be sensitive at the upper end of the band to a decrease in feed gain. The resulting S-parameters, normalized to 50 Ω, in Figure 5.16 show reflection better than −10 dB across the band.

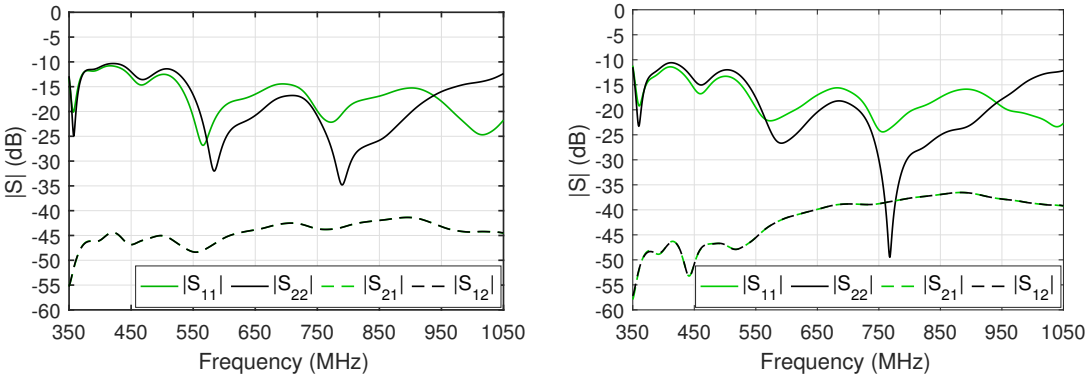

Figure 5.16: Reflection and coupling coefficients for the Sep2015 feed with 50 Ω coaxial lines. $|S_{11}|$ is reflection at port 1 (vert. polarization) and $|S_{21}|$ is the coupling to port 2. $|S_{22}|$ is reflection at port 2 (horiz. polarization) and $|S_{12}|$ is the coupling to port 1. Left: EM design; Right: Mechanical design. Resolution: < 1 MHz

5.2.3.2 Beam Pattern

In Figure 5.17 beam patterns in E-, D- and H-plane of the Sep2015 is exemplified for three frequencies, for both co- and cross-polarization. The symmetry is good between the polarizations (as expected), where x-polarization is represented by vertical polarization on-dish and y-polarization is represented by horizontal. The feed gain across the band ranges between $10.6 - 13.0$ dBi.

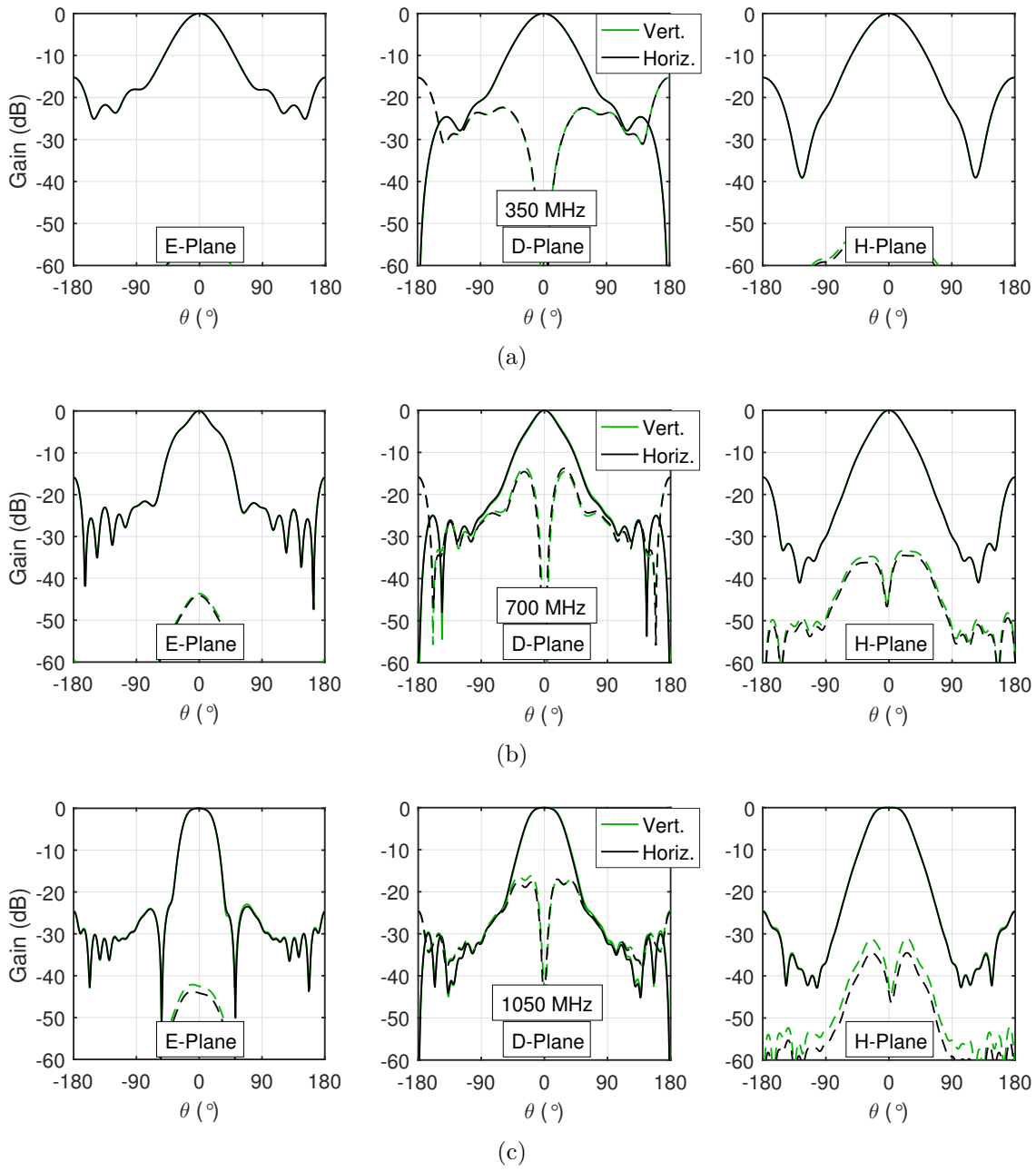

Figure 5.17: Simulated beam patterns for the Sep2015 feed in (left) E-, (middle) D- and (right) H-Plane. Green represents vertical polarization (port 1) and black represents horizontal polarization (port 2) with co-polar as solid and cross-polar as dashed lines. (a) 350 MHz. (b) 700 MHz. (c) 1050 MHz.

5.2.4 Feed Performance on Dish

In this section we show the simulated performance of the feed on the dish. We focus on the properties already mentioned and the requirements specified.

5.2.4.1 Positioning on Dish

To optimize performance on the dish, the feed is placed relative to the dish focal point so that the phase efficiency is maximized. In principle this means "snapping" the horn so that the dish focal point is in optimal alignment to the phase center of the horn. The snapping point Δ_{sp} is defined from the horn aperture rim moving inside the horn. The preferable Δ_{sp} should give the highest average sensitivity across the band and keep a physical margin so that the feed is not blocking the incoming rays from the MR to the SR. The inclusion of assembly margins is important to give a reasonable assembly tolerance. Therefore the Δ_{sp} is chosen not at the absolute maximum sensitivity average but rather close to it, where there is a margin between the feed and the active area of the dish. In Figure 5.18(b) we see the result of a set of simulations to find the optimal Δ_{sp}. The feed was simulated with 5 mm steps moving the focus of the dish further in to the feed to find a maximum average sensitivity. With a required average level of at least 4.2 m^2/K, an acceptable snapping point is found between 260 mm and 400 mm. Close to $\Delta_{sp} = 300$ mm the sensitivity level is clearly above the required and by ray tracing we can estimate that there is still a good margin between the feed rim and the active path in the dish at this location. In the system simulator software there is a routine that calculates optimal snapping point to maximize the phase efficiency. Results from this routine gives a similar point, close to $\Delta_{sp} = 300$ mm. We note that the aperture efficiency average also is maximized at $\Delta_{sp} = 300$ mm in Figure 5.18(a). The simulations indicate that small misalignment relative $\Delta_{sp} = 300$ mm in the optical direction could be allowed without a drastic decrease in performance. Therefore, an acceptable snapping point including tolerances could be given as $\Delta_{sp} = 300 \pm 10$ mm for feed performance on dish according to requirements and without risking physical blockage.

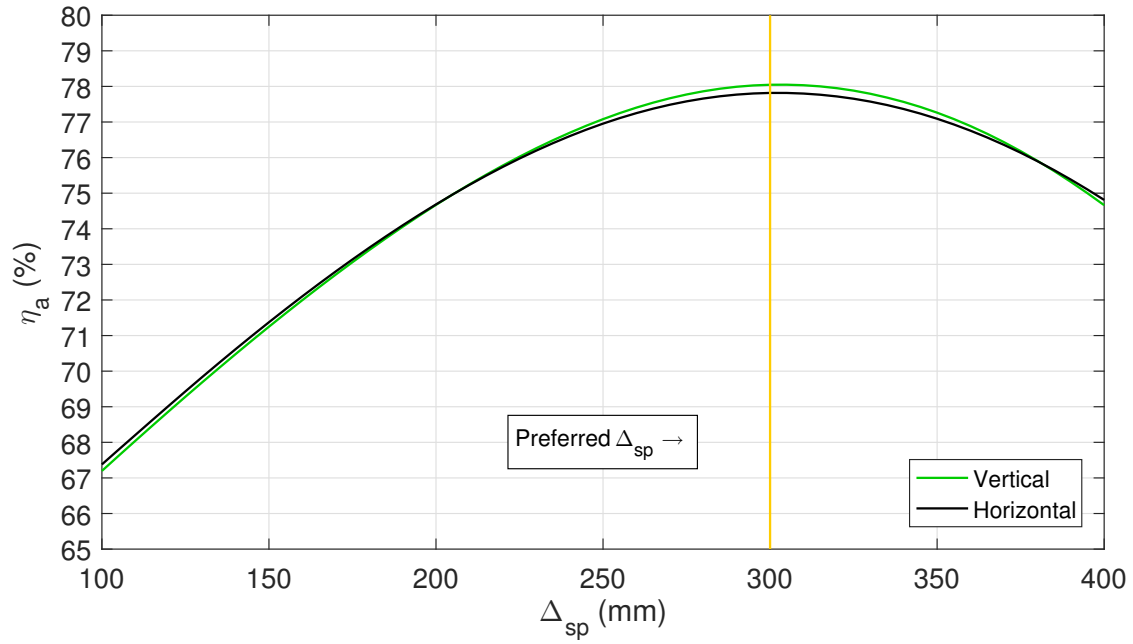

(a)

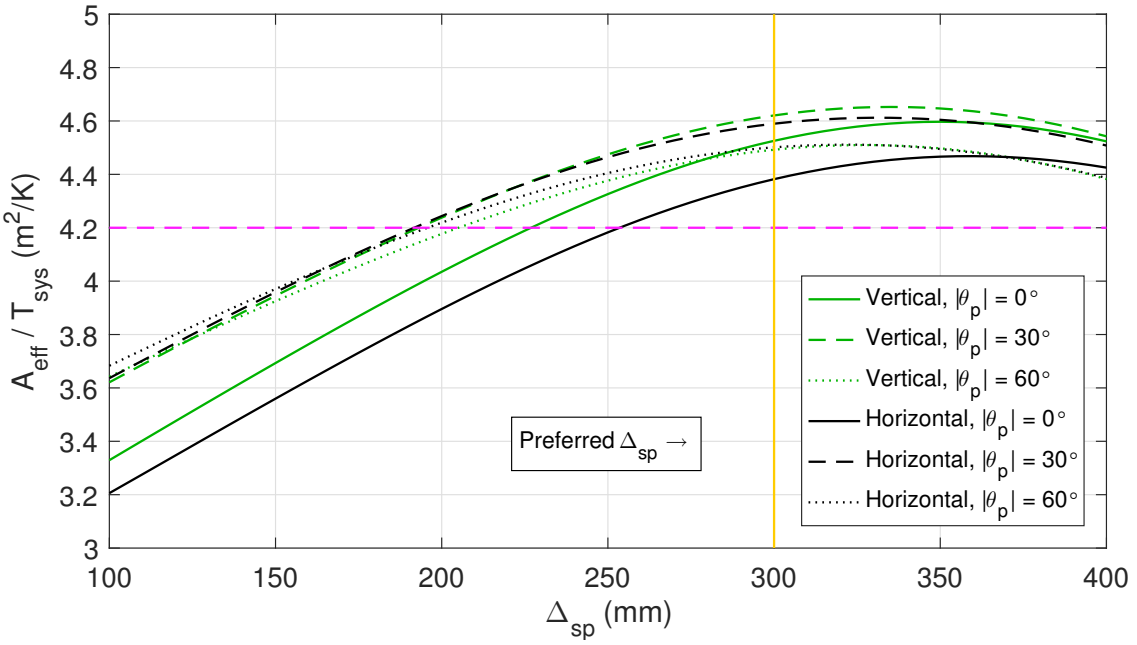

(b)

Figure 5.18: Optimization of Δ_{sp} for Sep2015 feed on the SKA dish; finding optimum feed location relative the dish focal point. (a) Average Aperture Efficiency. (b) Average Sensitivity. Both vertical (port 1) and horizontal (port 2) polarization are shown, sensitivity show zenith angle $|\theta_p| = 0°$ (zenith) down to $|\theta_p| = 60°$ (30° over the horizon). Purple dashed line represents 4.2 m^2/K requirement. Each average is calculated over the entire band using 15 frequency points. Resolution: 5 mm.

5.2.4.2 Cross Polarization

The cross-polarization levels within −1 dB and −3 dB contour of the main beam, normalized relative to the corresponding co-polarization, seen in Figure 5.19(a). The intrinsic cross-polarization ratio (IXR) is shown in Figure 5.19(b) and fulfill the requirement to be better than 15 dB.

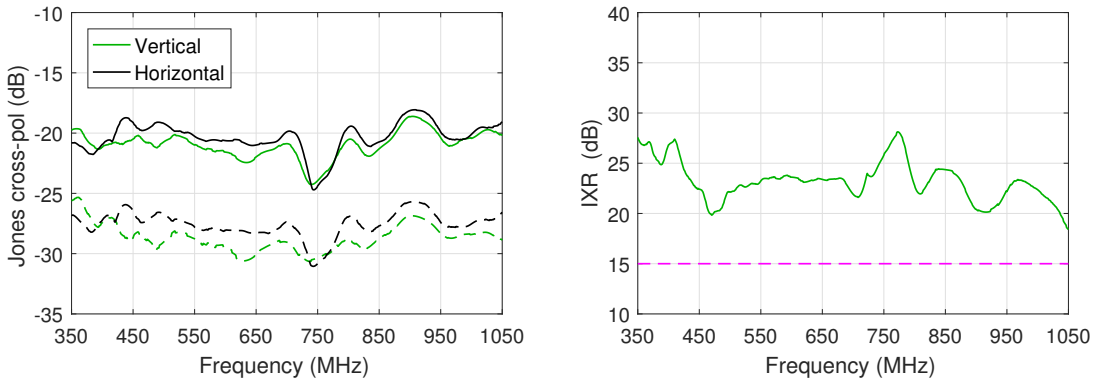

(a) (b)

Figure 5.19: Cross-polarization for Sep2015 feed on the SKA dish. Left: Jones cross-pol maximum within -1 dB contour (dashed) and within -3 dB contour (solid) of the main beam; Right: Minimum IXR within half power beam width. Plot resolution: 1 MHz.

5.2.4.3 Aperture Efficiency

The simulated aperture efficiency achieved with the Sep2015 design on the SKA dish is shown with 1 MHz resolution in Figure 5.20. The average value across the band is above 77 %, with a minimum of 70 % for the majority of the band, this is good performance for a 3 : 1 bandwith feed. For the span 500 − 975 MHz the efficiency is above 75 % which is considered a high level. Aperture efficiency show a continuously stable level across the band with no major drops. This has been an important focus of the project, since early models showed severe drops at certain frequencies which was most likely due to trapped modes in the feed. The deviations between the two polarizations at lower frequencies is related to the asymmetry in the offset dish structure, which also translates into different spill-over levels.

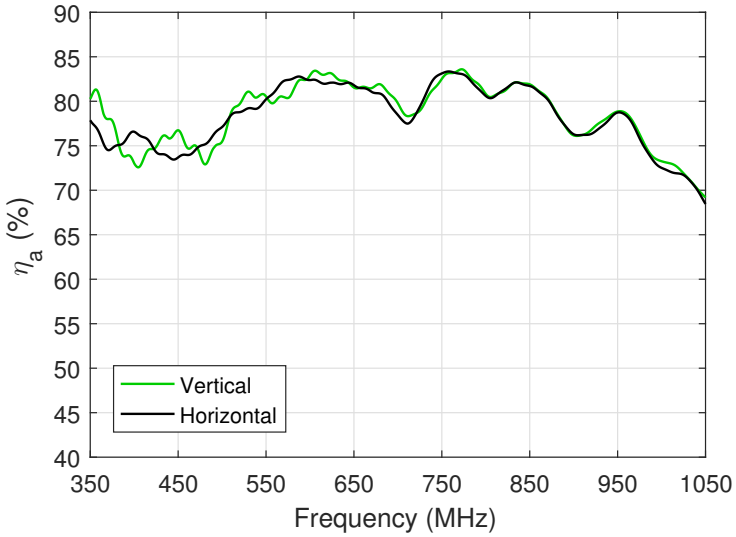

Figure 5.20: Simulated aperture efficiency, η_a, for Sep2015 feed on the SKA dish, vertical (port 1) and horizontal (port 2) polarization. Resolution: 1 MHz.

5.2.4.4 System Noise Temperature

The total system noise, T_{sys}, is shown for both polarizations in Figure 5.21 as the sum of the receiver temperature, T_{rec}, and the antenna temperature, T_A. Given a high total radiation efficiency this approximation is valid, as seen in Equation 2.27. T_{rec} is measured data for amplifiers, feed and back-end whereas T_A is calculated, according to Equation 2.25, with a given model of the sky temperature, as exemplified in Equation 2.24.

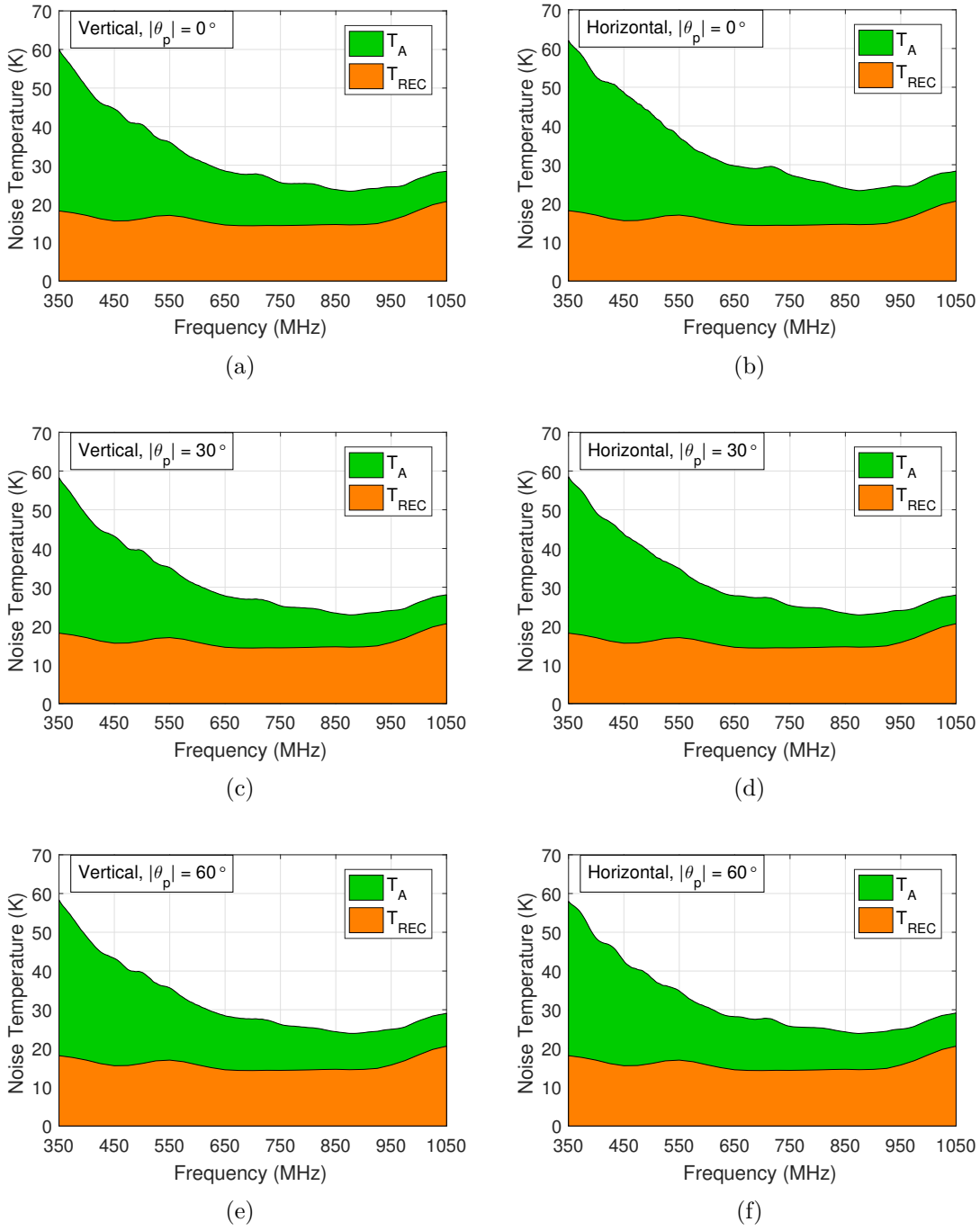

Figure 5.21: Simulated total system noise temperature, $T_{sys} \approx T_A + T_{REC}$, for the Sep2015 feed on the SKA dish. Left: Vertical polarization (port 1). Right: Horizontal polarization (port 2). (a)-(b) Zenith angle $|\theta_p| = 0°$ (zenith). (c)-(d) Zenith angle $|\theta_p| = 30°$. (e)-(f) Zenith angle $|\theta_p| = 60°$. Resolution: 1 MHz.

5.2.4.5 Sensitivity

The sensitivity, A_{eff}/T_{sys}, for the Sep2015 feed on the SKA dish is the main figure of merit for this system. With the estimated total system noise seen in Figure 5.21, the average sensitivity reaches well above the required 4.2 m^2/K for all relevant zenith angles on the telescope (see Figure 5.18(b)). In Figures 5.22(a), 5.22(c) and 5.22(e) simulated sensitivity over the band, with 1 MHz resolution, is shown for three telescope zenith angles, from $|\theta_p| = 0°$ (zenith) down to $|\theta_p| = 60°$ (30° over the horizon). At low frequencies the sensitivity drops below the required level (purple dashed line) for $|\theta_p| = 0°$, horizontal polarization in Figure 5.22(a). It is clear from the antenna noise temperature in Figure 5.22(b) that the sensitivity drop between $450 - 475$ MHz is due to increased spill-over pickup from the ground for the horizontal polarization. This can also be seen in the total system noise in Figures 5.21(a) – 5.21(b) for the two polarizations. The spill-over increase is a result of the over-illumination of the dish at these frequencies. Since the spill-over is calculated from the entire sphere, increased zenith angles could give a lower spill-over contribution due to more side-lobes being terminated on the cold sky compared to the ≈ 290 K ground. This can be seen in Figures 5.22(d) and 5.22(f) as the antenna noise temperature is at similar level for both polarizations unlike zenith in Figure 5.22(b).

Sensitivity requirement is set to a linear increase from at least 2.1 m^2/K at 350 MHz to at least 4.2 m^2/K at 650 MHz due to the large contribution of sky noise in T_A at these frequencies, see Figures 5.21(a) – 5.21(f). As an example, looking at 350 MHz for $|\theta_p| = 0°$, horizontal polarization we see that T_A is 70 % (≈ 43.9 K) of T_{sys}, at 650 MHz we have T_A close to 50 % (≈ 15.2 K) of T_{sys}. Because of the sky noise dominating the T_{sys} for $350 - 650$ MHz, it is reasonable to set a lower required sensitivity level. The linear increase corresponds to the fact that the sky noise decreases almost linearly from 350 to 650 MHz.

In general we have an increase of sky noise contribution to T_A across the band with larger zenith angle. This is intuitively explained by the fact that when the telescope is pointing closer towards the horizon, the amount of atmospheric mass the beam "sees" is increased compared to pointing in zenith direction. This is an unavoidable source of noise added to the system.

The feed shows high sensitivity performance with peaks at 6 m^2/K and continuous high level stability across the band. In Figure 5.23 it is exemplified for three frequency points that the sensitivity is stable from zenith down to $|\theta_p| = 60°$ which was the aim (stability goes beyond that). After further development, not included in this thesis, we have been able to decrease spill-over further at the lower and the higher end of the band to fulfill and exceed the requirement for all zenith angles, this is mentioned briefly in Section 6.1.

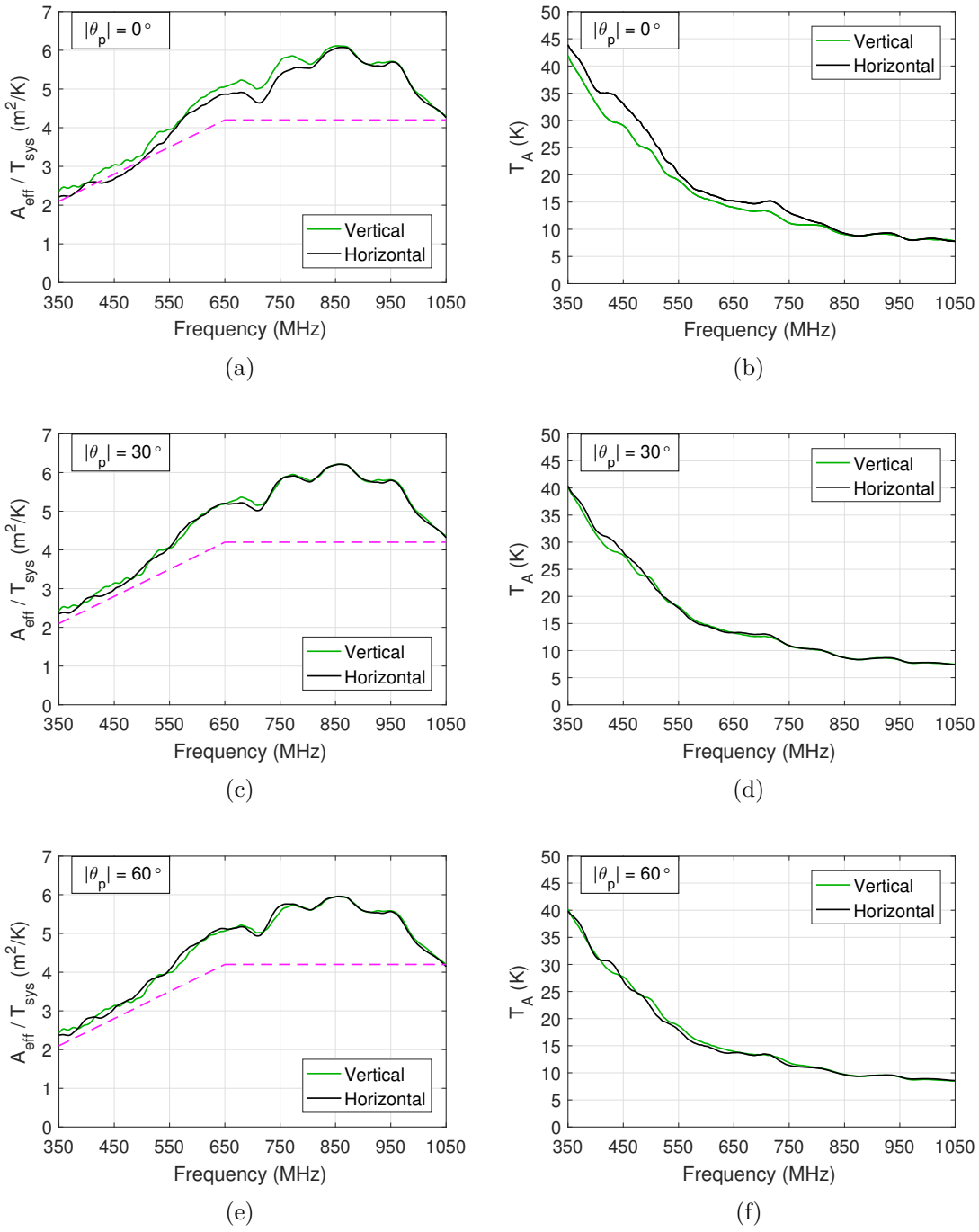

Figure 5.22: Simulated sensitivity (left), A_{eff}/T_{sys}, and antenna noise temperature (right), T_A, over frequency for Sep2015 feed on the SKA dish, vertical (port 1) and horizontal (port 2) polarization. (a)-(b) Zenith angle, $|\theta_p| = 0°$ (zenith). (c)-(d) Zenith angle, $|\theta_p| = 30°$. (e)-(f) Zenith angle, $|\theta_p| = 60°$. Resolution: 1 MHz.

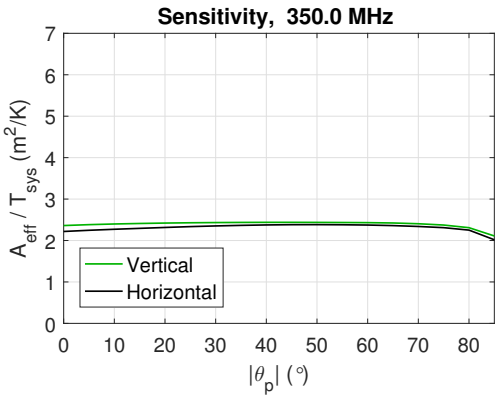

(a)

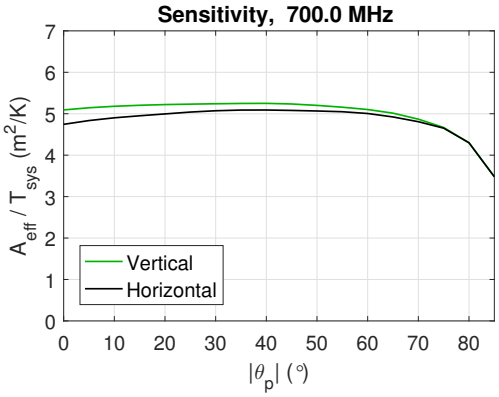

(b)

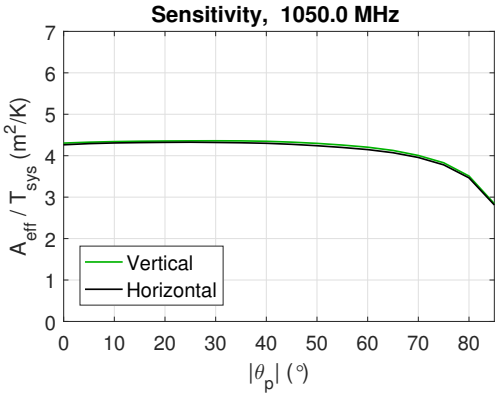

(c)

Figure 5.23: Simulated sensitivity, A_{eff}/T_{sys}, over zenith angle for Sep2015 feed on the SKA dish, vertical (port 1) and horizontal (port 2) polarization. (a) Frequency, 350 MHz (b) Frequency, 700 MHz (c) Frequency, 1050 MHz. Resolution: 5°.

5.2.4.6 Far-out Side-lobes

In Figure 5.24 simulated beam patterns on the SKA dish at frequencies 350 MHz and 1050 MHz are exemplified. The area between the solid red line and the dashed purple line indicate the 0 dBi to 6 dBi area. We fulfill the requirement of no side-lobes above the 6 dBi line, outside of $\theta = \pm 10°$ or the 8^{th} null, for all frequencies.

The second requirement of a total solid angle less than 0.05 steradian for side-lobes above 0 dBi outside $\theta = \pm 10°$ for all ϕ, is also fulfilled and illustrated in Figure 5.25. These are important requirements to avoid unwanted interference from sources located away from boresight.

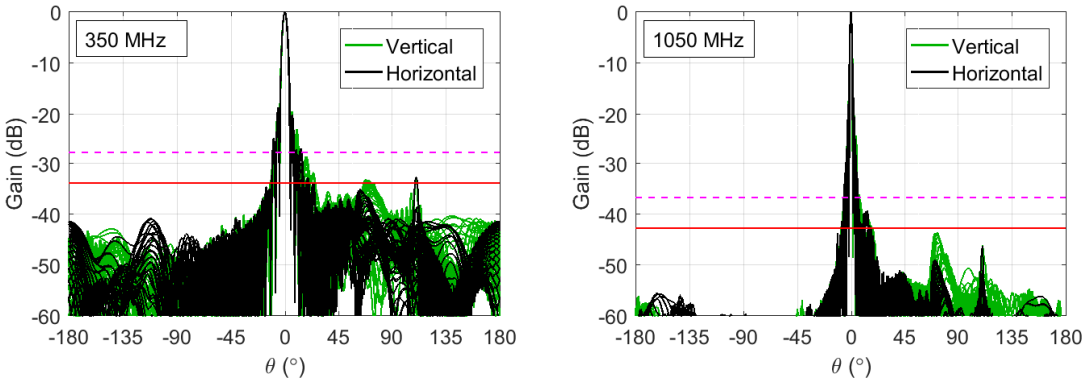

(a) (b)

Figure 5.24: Simulated beam patterns over all θ and ϕ for Sep2015 feed on the SKA dish, vertical (port 1) and horizontal (port 2) polarization. Solid red line defines 0 dBi (Gain), dashed purple line represents the 6 dBi far-out side-lobe specification limit. (a) Frequency, 350 MHz (b) Frequency, 1050 MHz. Resolution: 5°.

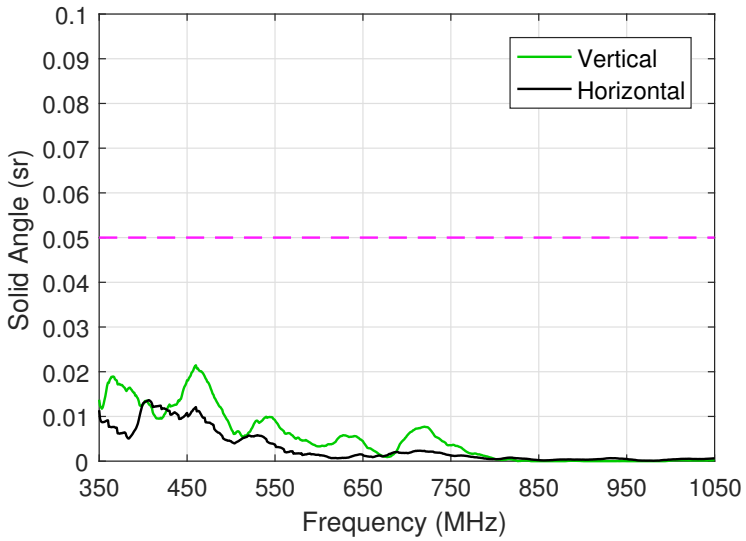

Figure 5.25: Total solid angle of side-lobe peaks above 0 dBi, for all θ and ϕ, outside $\theta = \pm 10°$ for Sep2015 feed on the SKA dish. Vertical (port 1) and horizontal (port 2) polarization. Resolution: 1 MHz.

5.2.5 Prototype and Measurements

The manufactured prototype was finished (including assembly) in early 2016 with great success, see Figure 5.26, details of this process will be left out. In June of 2016

the prototype was tested at the Dominion Radio Astrophysical Observatory located in Penticton, B.C., Canada and operated by the National Research Council Canada (NRC). Both hot-cold tests for receiver noise estimation, see Figure 5.28, and tests on dish were performed. The feed was mounted and connected to the DVA-1, an early prototype reflector for the SKA, also offset Gregorian type. Most of these data are at the time of this thesis still under processing and will not be featured, but we expect good agreement with our simulated results. S-parameter analysis at Onsala was performed with a network analyzer, and is seen to show reasonable agreement to simulated results in Figure 5.27, the unused port was terminated with 50 Ω. Deviations here are due to the precision of the manufactured parts, but for this prototype they are good enough. At 11.30 AM Pacific Standard Time (PST) on the 22nd of June 2016, we received first light with a sweep over the radio source Cassiopeia A with the feed mounted on the DVA-1, see Figure 5.29.

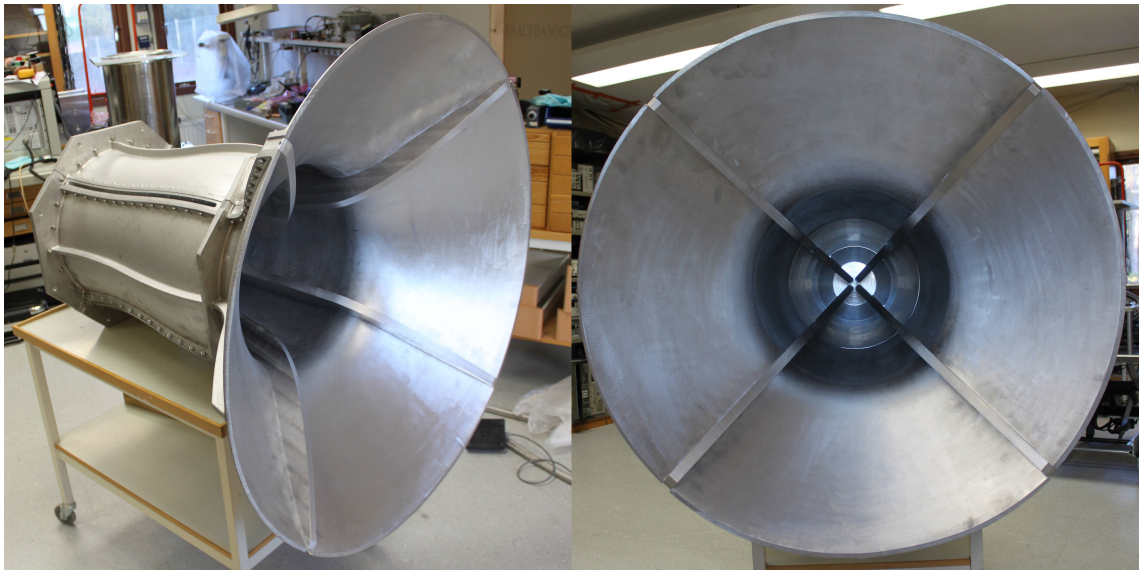

Figure 5.26: Sep2015 feed prototype. (Left) Perspective View, (Right) Top View.

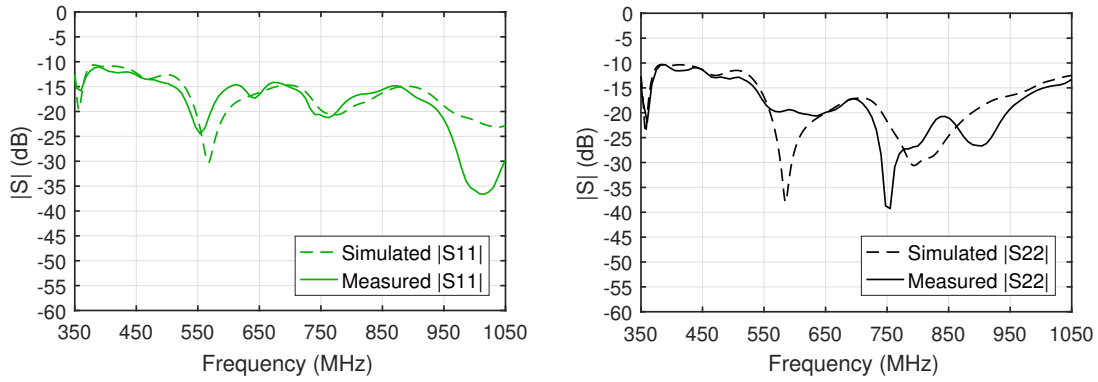

(a) (b)

Figure 5.27: Simulated and measured reflection over frequency for the Sep2015 feed. (a) Port 1 (vert. pol.) (b) Port 2 (horiz. pol.). Resolution: < 1 MHz.

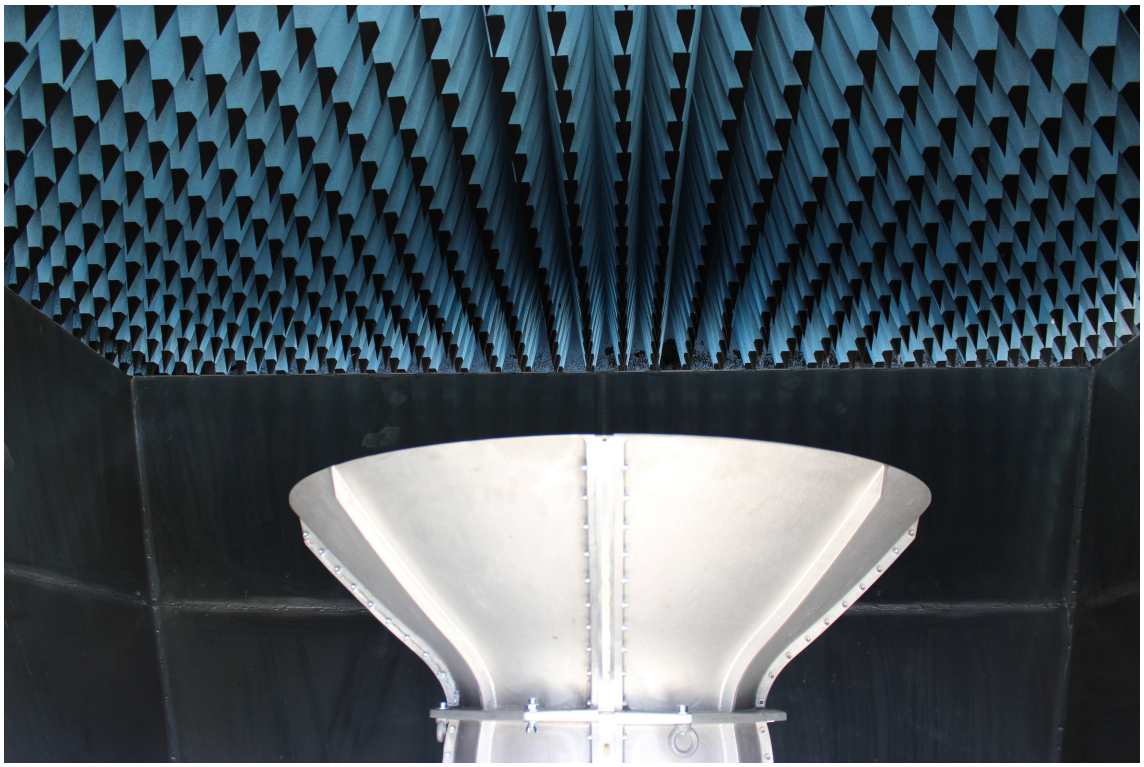

Figure 5.28: The Sep2015 feed prototype in the hot-cold facility (HCF) at DRAO.

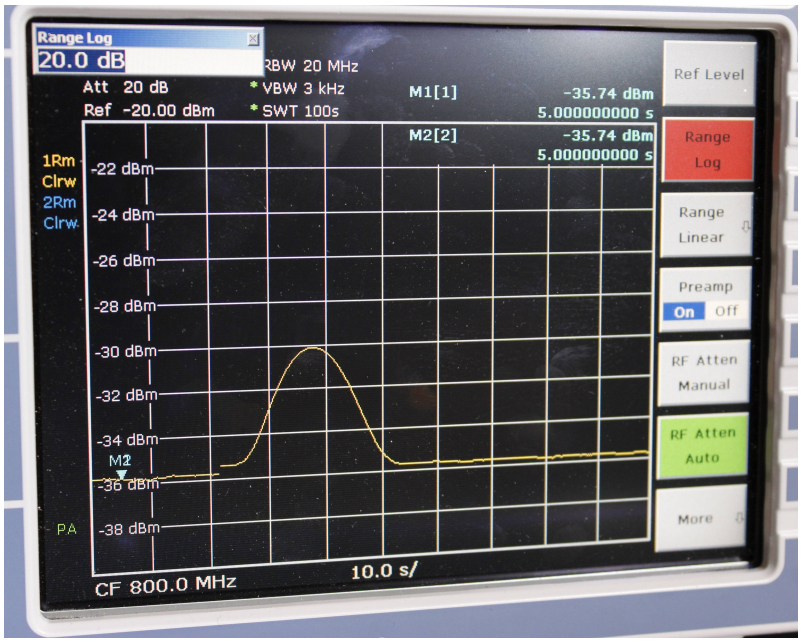

Figure 5.29: The Sep2015 feed prototype received first light on DVA-1 at 11.30 AM Pacific Standard Time (PST) on the 22nd of June 2016. The peak shows a sweep over Cassiopeia A at 800 MHz.

Figure 5.30: The Sep2015 feed prototype mounted on the DVA-1 dish at the DRAO site, Penticton, B.C., Canada. The feed is seen just underneath the SR.

6
Conclusions

We have proposed a $3:1$ wideband QRFH feed for the SKA Band 1 frequencies of $350-1050$ MHz. The design offers a high aperture efficiency averaging 77 % over the band with input reflection less than -10 dB. Optimization gives a low spill-over contribution to the total system noise and a minimum average sensitivity, A_{eff}/T_{sys}, close to 4.4 m^2/K across the band, well above the required 4.2 m^2/K. We also present a scaled QRFH feed for the frequencies $1.5-4.5$ GHz which lay the foundation for this work.

The feed optimization was performed with a specialized software toolbox ([11],[12]) utilizing CST and GRASP, where PSO and GA were implemented. Throughout the thesis, we emphasize how important the minimization of the unwanted noise, especially spill-over, is for the performance of the antenna system. The highly customizable QRFH spline profile gives great possibilities to tailor a feed to a specific dish. We concluded that this approach gave us more flexibility than for example the exponential profile [paper A.1] which has a smaller parameter space. This of course puts emphasis on a time efficient iteration evaluation, as more parameters are needed in the spline model. Due to the offset dish geometry, it is beneficial with a direct evaluation of the feed optimization process for each iteration in the system simulator. A different approach could have been to develop the feed for the supposed dish in CST alone. The noise estimation would then be intermediate evaluations, which of course could introduce unforeseen results when actually evaluated on the dish. This could lead to lost time in the optimization process.

Due to the system oriented nature of the project, the fitness functions used for iteration evaluation was weighted for on-dish performance. The most effort was put in to finding an optimization trade-off between high aperture efficiency and high sensitivity. Since these properties are highly dependent of each other, and their incorporated efficiencies, the setup for weighting this was a large part of the early process of the project. An over-weighted fitness function could easily get stuck in a local minimum, as where an under-weighted function could oscillate without reaching an acceptable performance level.

We have shown both through the scaled prototype and the full-scale Band 1 prototype, the possibility of manufacturing these designs. The technology transfer from electromagnetic design to a prototype CAD-model is proven possible. Manufactured feeds have been tested in both laboratory environment through an anechoic chamber, and on-dish (DVA-1) at the DRAO site in Penticton, B.C., Canada. At 11.30 AM Pacific Standard Time (PST) on the 22$^{\mathrm{nd}}$ of June 2016, the full-scale Band 1 feed received first light on DVA-1 with a sweep over the radio source Cassiopeia A.

6.1 Future Work

To limit this thesis, a lot of work done has intentionally been left out. The full-scale feed model presented, has since the time of prototyping been further optimized and the performance enhanced especially at the high and low end of the band. We have managed to increase the illumination efficiency and therefore the aperture efficiency, without sacrificing the spill-over performance. The spill-over contribution to the noise has also been reduced. Major parts of the advanced model development have included studies in

- Tolerance analysis of the feed for manufacturing purpose. Crucial dimensions of the feeding section of the horn are important to specify before manufacturing, to reach the desired performance. Since the frequencies are relatively low, the radiation performance is affected very little by small surface deviations (millimetre) in the flare and ridge. The contacting between the ridges and the horn itself however, remains important.
- Further tolerance analysis of the mounting position relative the dish focal point. Parts of this is presented in the thesis as mounting tolerances.
- Weight reduction analysis, where ways to preserve the electromagnetic performance while making the feed lighter has been investigated for obvious reasons.
- Noise source development for calibration of the receiver noise when mounted on the telescope.

References

[1] A. Unsöld and B. Baschek, *The New Cosmos: An Introduction to Astronomy and Astrophysics.* 5th Edition, Germany: Springer-Verlag Berlin Heidelberg, 2002, ISBN 978-3-662-04356-1.

[2] H. C. King, *The history of the telescope.* NY, USA: Dover Publications, 1955, ISBN 978-0-486-43265-6.

[3] A. R. Thompson, J. M. Moran, G. W. Swenson, Jr, *Interferometry and Synthesis in Radio Astronomy.* 2nd Edition, Germany: Wiley-VCH, 2001, ISBN 978-0-471-25492-8.

[4] SKA Organisation. *Square Kilometre Array.* (2016, Nov., 16) [Online]. Available: https://www.skatelescope.org/.

[5] NASA/ESA. *The Hubble Telescope.* (2016, Nov., 16). [Online]. Available: http://www.hubblesite.org/.

[6] P. Dewdney. (2013). *SKA1 system baseline design.* (2016, Nov., 16) [Online]. Available: https://www.skatelescope.org/wp-content/uploads/2014/11/SKA-TEL-SKO-0000002-AG-BD-DD-Rev01-SKA1_System_Baseline_Design.pdf. pp. 13-17.

[7] Onsala Space Observatory. *Onsala Space Observatory.* (2016, Nov., 16) [Online]. Available: http://www.chalmers.se/en/centres/oso/Pages/default.aspx.

[8] EMSS. *EMSS.* (2016, Nov., 16) [Online]. Available: http://www.emss.co.za/

[9] A. Akgiray, S. Weinreb, W. Imbriale, and C. Beaudoin, "Circular quadruple-ridged flared horn achieving near-constant beamwidth over multioctave bandwidth: Design and measurements," *IEEE Transactions on Antennas and Propagation*, vol. 61, no. 3, pp. 1099 – 1108, March, 2013.

[10] B. Billade, J. Flygare, M. Dahlgren, B. Wästberg, and M. Pantaleev, "A Wideband Feed System for SKA Band 1 Covering Frequencies From 350 - 1050 MHz," in *Proceedings of 10th European Conference on Antennas and Propagation (EuCAP2016).*, Davos, Switzerland, April 10-15, 2016, pp. 1-3.

[11] M. Ivashina, C. Bencivenni, O. Iupikov, and J. Yang, "Optimization of the 0.35-1.05 GHz Quad-Ridged Flared Horn and Eleven Feeds for the Square Kilometer

Array Baseline Design," in *Proceedings of 2013 International Conference on Electromagnetics in Advanced Applications (ICEAA2014),* Aruba, 9-13 Aug., 2014, pp. 513-516.

[12] M. Ivashina, O. Iupikov, R. Maaskant, W. van Cappellen, and T. Oosterloo, "An optimal beamforming strategy for wide-field surveys with phased-array-fed reflector antennas," *IEEE Transactions on Antennas and Propagation*, vol. 59, no. 6, pp. 1864 – 1875, June, 2011.

[13] MathWorks Inc. *MATLAB.* (2016, Nov., 18) [Online]. Available: http://www.mathworks.com/products/matlab.

[14] Computer Simulation Technology. *CST Microwave Studios.* (2016, Nov., 18) [Online]. Available: https://www.cst.com/products/CSTMWS.

[15] TICRA. *GRASP.* (2016, Nov., 18) [Online]. Available: http://www.ticra.com/products/software/grasp.

[16] Altair Engineering Inc. *FEKO.* (2016, Nov., 18) [Online]. Available: https://www.feko.info/.

[17] Ansys Inc. *HFSS.* (2016, Nov., 18) [Online].
Available: http://www.ansys.com/products/electronics/ansys-hfss.

[18] P-S. Kildal. *Foundation of Antennas: A Unified Approach for Line-Of-Sight And Multipath.* 2014 Edition. Sweden: Kildal Antenn AB, 2014, ISBN 978-1-608-07867-7 (2015 Edition).

[19] T. A. Milligan. *Modern Antenna Design.* 2nd Edition. NJ, USA: Wiley-IEEE Press, 2005, ISBN 978-0-471-45776-3.

[20] S. K. Sharma, S. Rao, L. Shafai. *Handbook of Reflector Antennas and Feed Systems, Volume 1: Theory and Design of Reflectors.* 1st Edition. MA, USA: Artech House, 2013, ISBN 978-1-608-07515-7.

[21] C. A. Balanis. *Antenna Theory: Analysis and Design.* 4th Edition. NJ, USA: Wiley, 2016, ISBN 978-1-118-64206-1.

[22] IEEE Antennas and Propagation Society, "IEEE Standard for Definitions of Terms for Antennas," *IEEE Standards* Rev. 145-2013.

[23] M.S. Nieman, "The Principle of Reciprocity in Antenna Theory," in *Proceedings of the IRE* vol. 31, no. 12, pp. 666 - 671, Dec., 1943.

[24] A.C. Ludwig, "The Definition of Cross Polarization," *IEEE Transactions on Antennas and Propagation,* vol. 21, no. 1, pp. 116 - 119, January, 1973.

[25] T. D. Carozzi, G. Woan, "A Fundamental Figure of Merit for Radio Polarimeters," *IEEE Transactions on Antennas and Propagation,* vol. 59, no. 6, pp. 2058

- 2065, June, 2011.

[26] P-S. Kildal, "Factorization of the Feed Efficiency of Paraboloids and Cassegrain Antennas," *IEEE Transactions on Antennas and Propagation,* vol. 33, no. 8, pp. 903 - 908, Aug., 1985.

[27] M. Wahde, *Biologically Inspired Optimization Methods: An Introduction.* UK: WIT Press, 2008, ISBN 978-1-84564-148-1.

[28] J. Kennedy and R. Eberhart, "Particle Swarm Optimization" in *Proceedings of IEEE International Conference on Neural Networks,* Perth, Australia, 27 Nov. - 1 Dec., 1995, vol. 4, pp. 1942 - 1948.

[29] M. Ivashina, R. Maaskant and B. Woestenburg, "Equivalent System Representation to Model the Beam Sensitivity of Receiving Antenna Arrays," *IEEE Antennas Wireless Propagation. Letter (AWPL)*, pp. 733-737, Oct., 2008.

A

Appended Papers

Paper A.1

A Wide-band Feed System for SKA Band 1 Covering Frequencies From 350 - 1050 MHz

B. Billade, **J. Flygare**, M. Dahlgren, B. Wästberg, and M. Pantaleev,
Proceedings of 10th European Conference on Antennas and Propagation (EuCAP2016).,
Davos, Switzerland, April 10-15, 2016, pp. 1-3.

A Wide-band Feed System for SKA Band 1 Covering Frequencies From 350 - 1050 MHz

Bhushan Billade[1], Jonas Flygare[1], Magnus Dahlgren [1], Bo Wästberg[1], Miroslav Pantaleev[1]
[1](Onsala Space Observatory): Dept. of Earth and Space Science, Chalmers University of Technology, Sweden
bhushan.billade@chalmers.se

***Abstract*—We present the design of a wideband feed system for the Band 1 of the Square Kilometer Array (project). The Band 1 feed system uses a quad-ridged flared horn (QRFH) optimized for a offset Gregorian dual reflector dish to cover RF frequencies from 350 - 1050 MHz, and a cryogenic low noise amplifier (LNA). The feed horn is optimized to achieve best A_{eff}/T_{sys} over the entire band, by making trade-off between aperture efficiency and spill over noise contribution.**

The optimised feed horn shows above 70% efficiency over the entire 3:1 band, with return loss better than 10 dB. The cryostat following the feed has between 9 to 14 K noise, measured at the co-axial connector of the QRFH. The estimated on-sky sensitivity of the feed system is better than specified 4.2 m^2/K averaged over the entire frequency band.

***Index Terms*—QRFH, Wideband feed, SKA, cryogenic feed systems.**

I. Introduction

The Square Kilometer Array (SKA) is a new radio interferometer currently at the end of its design phase, the telescope aims to have total effective collecting area of one square kilometer, making it worlds biggest and most sensitive radio telescope at these frequencies. The project is an international effort to built world's largest radio telescope, involving 10 member countries. The telescope would cover frequencies from 50 MHz to 13.8 GHz, divided into SKA-low, SKA-survey, and SKA-mid [1]. The division is based on the technology that would be used in particular frequency bands. The SKA-low would use a low frequency aperture array operating from 50 - 350 MHz, the SKA-survey would use phased array feeds in a dual reflector system operating from 350 MHz to 4 GHz, and the SKA-mid would use five wide band single pixel feed systems to cover frequencies from 350 MHz to 13.8 GHz.

The work presented here concerns the development of feed system for the Band 1 of the SKA-mid. The Band 1 feed system is designed to cover RF frequencies from 350 - 1050 MHz. The SKA-mid Band 1 consists of a QRFH operating at room temperature, followed by a cryogenic LNA at 20 K ambient temperature.

II. Band 1 system overview

The SKA Band 1 Feed Package uses a Quad-Ridged Flared Horn (QRFH) at ambient temperature and cryogenically cooled LNAs. The performance of the QRFH in the different optics designs considered for SKA are described in the optics analysis report [2]. The QRFH was selected after comparing cost and performance aspects with the Eleven Feed, the other feed considered as possible candidate for Band 1 [3].

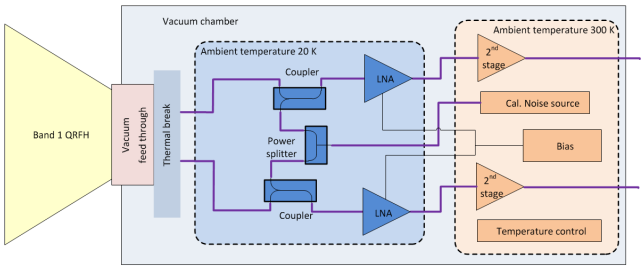

Fig. 1. Overview of Band 1 feed system.

Fig. 1 shows the design concept for the Band 1 feed system. The QRFH is placed at room temperature and attached mechanically to the front plate of the cryostat. The RF interface to the signal chain is provided by vacuum feed through connectors at the input of the cryostat. The heat transfer from 300 K to 20 K cold stage is minimised using stainless steel coaxial cables to transport the signal. These cables are anchored thermally at 20 K and 70 K. The RF signal for each of the two orthogonal polarisation then passes though a directional coupler where calibration noise signal is injected, followed by a cryogenic LNA and 2nd stage LNA. The cryogenic LNAs and direction coupler are attached to the 20 K cold stage of the cryostat. The 2nd stage LNAs, and calibration noise source are located at the 300 K stage.

III. Cryostat design

Fig. 2 shows a cross section of the Band 1 cryostat, which uses a Gifford-McMahon (GM) cooler. The LNAs and the directional couplers are placed on thermally stabilized copper plate that is attached to the 20 K stage of the cryo-cooler using weak thermal links. A stainless steel (SS) co-axial cable is used between the vacuum feed through located at 300 K interface and the direction coupler at 20 K, to reduces the thermal heat flow. Since the SS co-axial cable is located before the first stage LNA, looses of the SS cable add significant noise to the overall system noise, therefore length of this cable is carefully optimized to reduce the added noise contribution but at the same time providing enough thermal isolation between the two temperature stages.

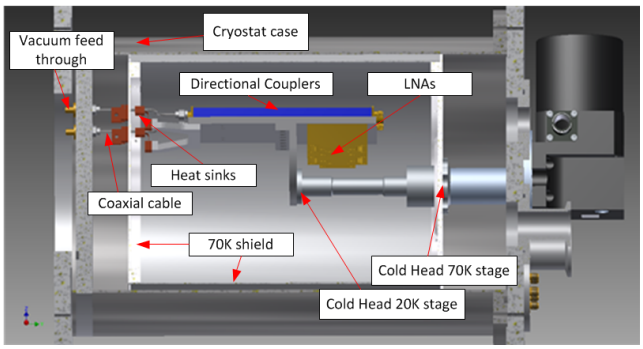

Fig. 2. Overview of Band 1 cryostat.

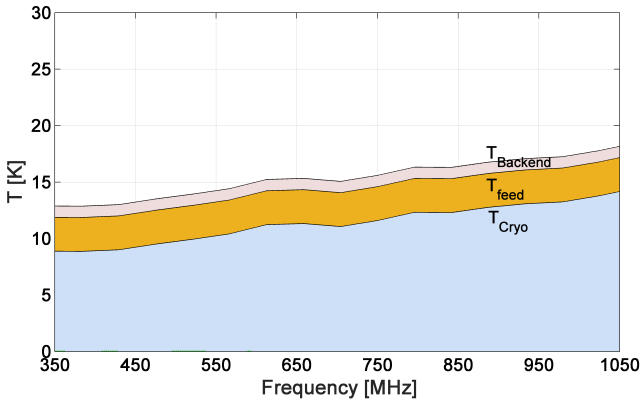

Fig. 3. Measured noise temperature of the receiver at the input of the horn.

Fig. 3 shows the expected noise temperature at the input of the feed horn, where T_{Cryo} is the noise temperature measured at the input of the cryostat which includes the cryogenic LNA, direction coupler and all the losses up to the 300 K interface of the cryostat. T_{feed} represents the estimated noise contribution from the feed at room temperature, and $T_{Backend}$ is the noise contribution from all the subsequent components after the first cold LNA.

IV. Feed Design

The QRFH for the Band 1 of the SKA-mid has been designed to maximise the overall sensitivity of the telescope, by making trade off between the aperture efficiency and spill over noise contribution over the entire band while keeping the feed input reflection coefficient in the acceptable range. Fig. 4 shows the Band 1 QRFH, both the ridge profile, and outer horn profile is defined using spline function. In our simulations we observed that a spline profile horn provide better efficiency compared to exponentially tapered QRFH over 3:1 band width. For wider bandwidths however, exponentially profile [4] might still provide better efficiency.

Fig. 5 shows the CST [5] simulation results of reflection coefficient of the QRFH for both the ports. For both the ports the input reflection is better than $-10\ dB$. The slight degradation in the input matching at the low end of the frequency band is believed to be associated with the ridge and horn profile, and not with feeding section. By modifying

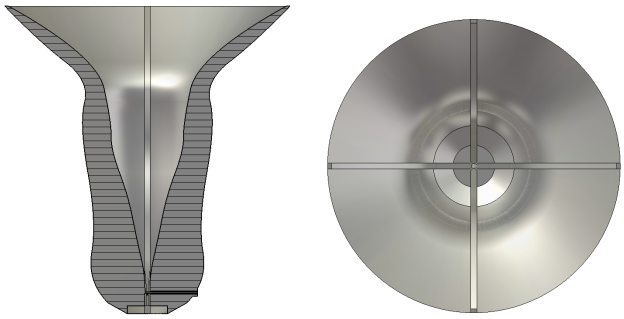

Fig. 4. SKA-mid Band 1 QRFH using spline profile for the flare and ridges.

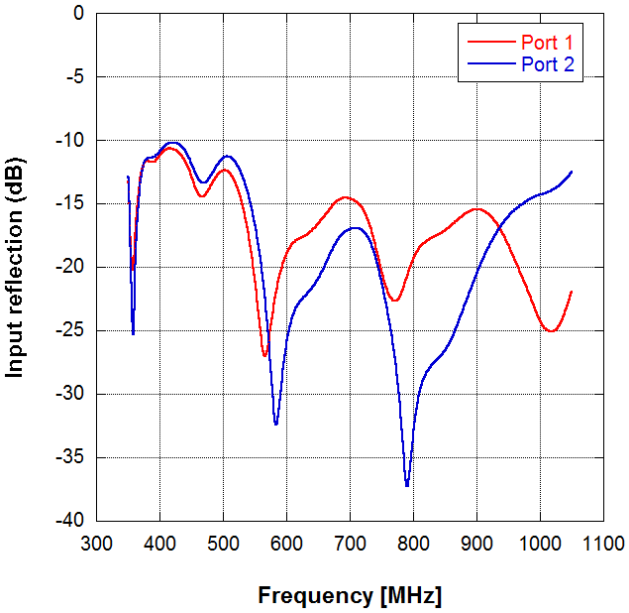

Fig. 5. Simulated reflection at the co-axil input line of the QRFH.

the ridge and horn profile input reflection can be improved, but we observe reduction in the overall efficiency. However, we believe that further optimisation of the feed could improve the input matching without substantially affecting the efficiency.

V. Analysis of the System Sensitivity

In order to accurately estimate the overall system sensitivity, one needs to accurately estimate the spill over noise contribution after the reflector system. The estimation of the overall on-sky sensitivity and optimisation of QRFH is done using a GRASP system simulator [6], where the CST far field patters are analysed in the SKA dish geometry in GRASP [7]. Fig. 6 shows the dish geometry used in the feed optimisation. SKA dish is a offset Gregorian geometry, the projected diameter of the primary reflector is 15 m, and the diameter secondary reflector is has 5 m, with extension on the bottom side to minimise the ground noise pickup in the feed spill over.

The simulated aperture efficiency of the QRFH in the SKA dual reflector geometry is shown in Fig. 7. For both the polarisations the aperture efficiency is better than 75% over

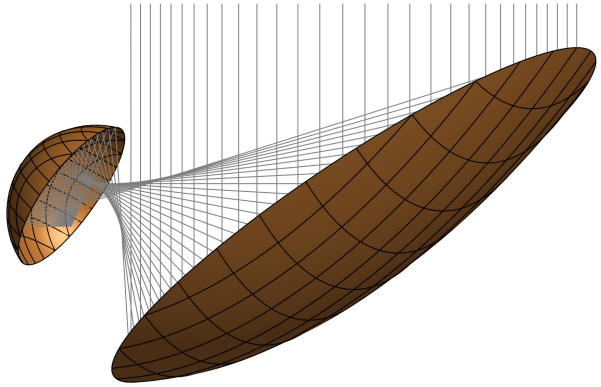

Fig. 6. Offset Gregorian dish geometry for the SKA.

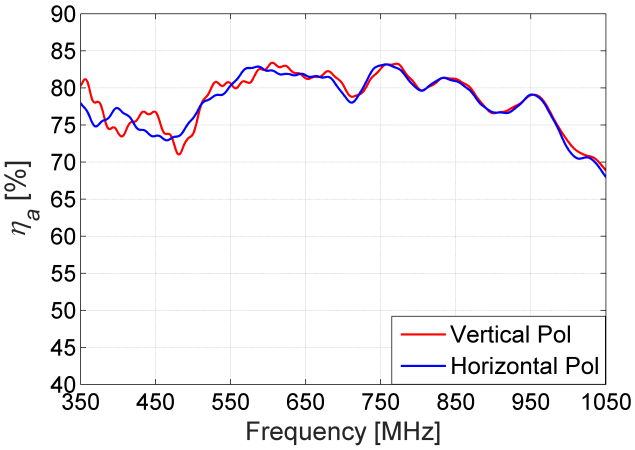

Fig. 7. Simulated aperture efficiency of the QRFH in the SKA dual reflector geometry.

most of the frequency band, and better than 70% over the entire band.

Fig. 8 shows the simulated system sensitivity of the feed in the SKA dish geometry, using the receiver noise estimation described in previous section, and the analysis from GRASP and system simulator. The sensitivity is calculated when the dish is looking at zenith, for other elevation angles the over all sensitivity changes as function of elevation angle.

VI. Conclusion

The current design of the Band 1 QRFH using a spline profile to define the ridges and horn, provides 75% efficiency in the offset Gregorian dual reflector SKA dish, with input reflection better than $-10\,dB$ over the entire frequency band. The overall Band 1 system with QRFH placed at room temperature and the cryogenic LNAs shows very promising results and estimated performance meets the sensitivity requirement of $4.2\,m^2/K$ averaged over the entire frequency band.

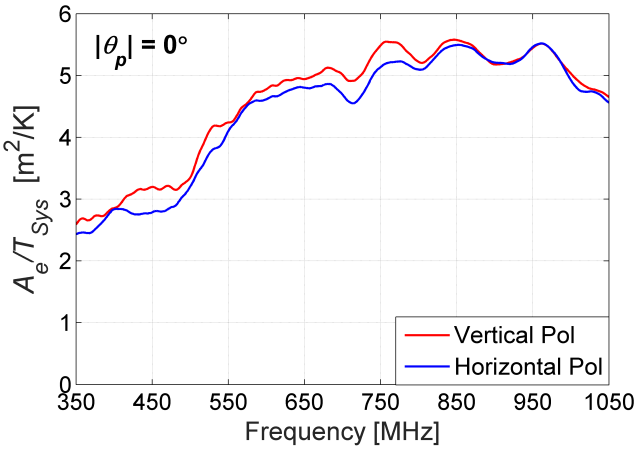

Fig. 8. Simulated dish sensitivity (A_{eff}/T_{sys}) of the QRFH in the SKA dish geometry.

Acknowledgment

This work has been funded by Swedish VR Research Infrastructures Planning Grant Swedish contributions to the SKA radio-telescope in its pre-construction phase. The system simulator was provided by Dr. Marianna Ivashina. The GRASP models for the SKA dish geometry, and preliminary spline QRFH model were provided by Dr. Isak Theron and Dr. R. Lehmensiek, EMSS Antennas, South Africa.

References

[1] P. Dewdney, "SKA1 system baseline design," pp. 1–98, March 2013 [Online]. Available: https://www.skatelescope.org/wp-content/uploads/2014/11/SKA-TEL-SKO-0000002-AG-BD-DD-Rev01-SKA1_System_Baseline_Design.pdf.

[2] R. Lehmensiek, "SKA optics options: SPF EM analyses," SKA organisation, Internal project document, Dec 2014.

[3] B. Billade, "Band 1 feed selection document, performance and cost study," SKA organisation, Internal project document, Oct 2014.

[4] A. Akgiray, S. Weinreb, W. Imbriale, and C. Beaudoin, "Circular quadruple-ridged flared horn achieving near-constant beamwidth over multioctave bandwidth: Design and measurements," *Antennas and Propagation, IEEE Transactions on*, vol. 61, no. 3, pp. 1099–1108, March 2013.

[5] CST, "CST MICROWAVE STUDIO," http://www.cst.com/Content/Products/MWS/Overview.aspx.

[6] M. Ivashina, O. Iupikov, R. Maaskant, W. van Cappellen, and T. Oosterloo, "An optimal beamforming strategy for wide-field surveys with phased-array-fed reflector antennas," *Antennas and Propagation, IEEE Transactions on*, vol. 59, no. 6, pp. 1864–1875, June 2011.

[7] TICRA, "GRASP," http://www.ticra.com/products/software/grasp.